

POLITECNICO DI TORINO

Master's Degree in Aerospace Engineering



Master's Degree Thesis

Efficient introduction of stiffness and density mistuning in the reduced order models of bladed disks

Supervisors

Prof. Stefano ZUCCA

Dr. Mehrdad POURKIAEE

Candidate

Giacomo SALETTI

October 2022

Abstract

This thesis focuses on a detailed implementation of the Relative Cyclic Component Mode Synthesis (RCCMS) approach on cyclically symmetrical systems with an in depth development of the algebra involved. Subsequently, it is showed how stiffness and density mistuning can be efficiently introduced in the final Reduced Order Models (ROMs). Eventually, numerical simulations are presented to reveal the accuracy of the RCCMS approach in predicting natural frequencies, mode shapes and linear forced response of the reduced systems of a bladed disk. In conclusion, the performances of the systems built with the two types of mistuning introduced are compared to show how, in some cases, density mistuning can be a valid alternative to stiffness mistuning.

Acknowledgements

Sono molte le persone che meritano un ringraziamento, prime fra tutti il Professor Stefano Zucca e il Dottor Mehrdad Pourkiaee che mi hanno mostrato come ci si approccia all'attività di ricerca e l'importanza dell'essere consistenti nel proprio lavoro.

Tante altre persone hanno contribuito a questa tesi, chi con consigli più tecnici e chi ascoltandomi pazientemente mentre cercavo di mettere ordine alle mie idee. Questi ultimi hanno avuto un ruolo fondamentale, più importante di quello che essi stessi pensano, dato che è stato in quei momenti di riflessione ad alta voce che spesso ho capito come risolvere il problema su cui mi arrovellavo in quell'istante.

Un ultimo sentito ringraziamento va a chi mi ha dato la possibilità di intraprendere il mio percorso universitario. È tutto fuorché scontata l'occasione di seguire le proprie aspirazioni e io sono veramente grato di averla avuta.

Table of Contents

List of Figures	VI
1 Introduction	1
1.1 Contextualization of the problem	1
1.2 Outline	3
2 Methodology	4
2.1 Reduction applied to a full bladed disk's system	4
2.2 Sector level calculations	9
2.3 Full stick modes	11
2.4 Constraint modes	16
2.5 Reduced matrix computation review	18
2.6 Mistuning introduction	18
2.6.1 Stiffness mistuning	18
2.6.2 Density mistuning	20
3 Results	22
3.1 Description of the models	22
3.1.1 FE model	22
3.1.2 Reduced order models	23
3.1.3 Mistuning patterns	24
3.2 Tuned system characteristics	28
3.3 Stiffness mistuning	29
3.3.1 Natural frequencies	29
3.3.2 Mode shapes	33
3.3.3 Linear forced response	37
3.4 Density mistuning	38
3.4.1 Natural frequencies	38
3.4.2 Mode shapes	41
3.4.3 Linear forced response	43
3.5 Performances comparison between density and stiffness mistuning	45

4	Conclusions	49
	Bibliography	50
A	Comparison of the stiffness and density mistuned systems	51
A.1	Natural frequencies	51
A.2	mode shapes	52

List of Figures

3.1	Full bladed disk	22
3.2	Elemental sector, (a) Shroud interface, (b) Disk interface	23
3.3	Example of tuned mode shape of the open contact system	26
3.4	Example of mistuned mode shape of the open contact system	26
3.5	Example of tuned mode shape of the close contact system	27
3.6	Example of mistuned mode shape of the close contact system	27
3.7	Natural frequencies at various harmonic indexes for the tuned systems	28
3.8	Deviation of the different tuned ROMs in predicting the natural frequencies	29
3.9	Natural frequencies of the open contact system, with 3% stiffness mistuning	30
3.10	Deviation between the natural frequencies (Ansys-ROM) of the open contact system, with 3% stiffness mistuning	30
3.11	Natural frequencies of the close contact system, with 3% stiffness mistuning	31
3.12	Deviation between the natural frequencies (Ansys-ROM) of the close contact system, with 3% stiffness mistuning	31
3.13	Comparison of the deviations between the 3% and 6% stiffness mistuned systems, open contact	32
3.14	Comparison of the deviations between the 3% and 6% stiffness mistuned systems, close contact	32
3.15	MAC plot for the open contact system with 3% stiffness mistuning .	33
3.16	MAC plot for the open contact system with 6% stiffness mistuning .	34
3.17	Normalized displacement of the chosen node in all sectors	35
3.18	MAC plot for the full stick system with 3% stiffness mistuning . . .	35
3.19	MAC plot for the full stick system with 6% stiffness mistuning . . .	36
3.20	Normalized displacement of the chosen node in all sectors, mode 25	36
3.21	Envelope of maximum response for the full stick system with 3% stiffness mistuning, $EO = 11$	37

3.22	Envelope of maximum response for the full stick system with 6% stiffness mistuning, $EO = 11$	38
3.23	Deviation between the natural frequencies (Ansys-ROM) of the open contact system, with 3% density mistuning	39
3.24	Deviation between the natural frequencies (Ansys-ROM) of the close contact system, with 3% density mistuning	39
3.25	Comparison of the deviations between the 3% and 6% density mistuned systems, open contact	40
3.26	Comparison of the deviations between the 3% and 6% density mistuned systems, close contact	40
3.27	MAC plot for the open contact system with 3% density mistuning	41
3.28	MAC plot for the open contact system with 6% density mistuning	42
3.29	MAC plot for the close contact system with 3% density mistuning	42
3.30	MAC plot for the close contact system with 6% density mistuning	43
3.31	Envelope of maximum response for the full stick system with 3% density mistuning, $EO = 11$	44
3.32	Envelope of maximum response for the full stick system with 6% density mistuning, $EO = 11$	44
3.33	Accuracy in predicting the natural frequencies of the open contact systems, considering different ROMs sizes	45
3.34	Accuracy in predicting the natural frequencies of the close contact systems, considering different ROMs sizes	46
3.35	Accuracy in predicting the mode shapes of the open contact systems, considering different ROMs sizes	47
3.36	Accuracy in predicting the mode shapes of the close contact systems, considering different ROMs sizes	47
A.1	Natural frequencies deviation between the stiffness and density mistuned open contact systems	52
A.2	Natural frequencies deviation between the stiffness and density mistuned closed contact systems	52
A.3	mode shapes comparison between the stiffness and density mistuned open contact systems	53
A.4	mode shapes comparison between the stiffness and density mistuned closed contact systems	53

Chapter 1

Introduction

1.1 Contextualization of the problem

Turbomachinery today plays a fundamental role in aviation both civil and military, but has also numerous terrestrial applications. Critical components of turbomachines are the bladed disks which are highly subjected to periodic stresses. This makes it essential to be able to predict their expected life before an eventual high cycle fatigue (HCF) failure. Accordingly, it is necessary to perform forced response analysis to efficiently compute the maximum response of the system in different conditions.

Forced response analysis become increasingly computationally demanding with the growth of the dimensions of the finite elements models, in order to overcome this issue, different techniques have been developed to reduce the size of the models without compromising the accuracy of the results of the analysis.

In an ideal condition, the cyclic symmetry of the bladed disks is guaranteed, this allows to perform linear and even non-linear analysis on reduced models built using only single sector computations. In reality though, the cyclic symmetry of the bladed disk is compromised by many factors like geometrical tolerances, material inhomogeneity, assembly process or due to the operating conditions such as the wear phenomena. This asymmetries of the system are collectively referred as mistuning. The presence of mistuning can have a strong impact on the dynamic of the system, in particular can cause vibration energy to be localized around few number of blades which can result in premature HCF of the blades.

Mistuning is usually divided in small and large. Small mistuning allows for the assumption that, considering a certain range of natural frequencies, mode shapes

of the mistuned bladed disks, in that range, can be considered a linear combination of the tuned bladed disk's mode shapes in the same frequencies range. When this assumption loses its validity then the mistuning is considered large.

To perform the analysis on a mistuned bladed disk, since it is impossible to use the full system due to the large number of degrees of freedom, it is necessary to build the reduced matrices of that system. The approach studied in this theses will use a technique based on Relative Cyclic Component Mode Synthesis (RCCMS) [1]. This method was tailored for nonlinear forced response analysis of bladed disks subjected to different sources of friction damping, but in this case, the focus will be on the introduction of different types of mistuning and the performances of the resulting ROMs in terms of linear forced response.

The ROMs built using RCCMS have numerous advantages for this study:

- The ROMs are built only from sector level calculations
- The ROMs include relative displacement between contact surfaces
- The method allows to introduce small mistuning directly in the final matrices

Using only sector level calculations is a requirement because it is computationally unsustainable to operate with the full system matrices.

Having retained relative displacements at contact surfaces allows to easily move between the two linear conditions of the system that will be considered: one with the contact interfaces completely clumped to each other and one with the two interfaces not interacting.

Finally having the possibility to introduce the mistuning in the final ROMs allows for a statistical characterization of the phenomena. The building process of the reduced matrices is, in fact, quite demanding and not being required to repeat the process for every mistuning pattern is really useful.

Small mistuning is usually introduced in terms of small deviations of a structural property of the system from its nominal value. In this theses will be studied how introducing the mistuning in terms of deviation of stiffness or density impact differently the accuracy of the ROMs and in particular, how and why the density mistuned ROMs can, in some cases, outperform the stiffness mistuned ones.

1.2 Outline

The theses is divided in the following chapters:

- **Chapter 2** describes the methodology to build the RCCMS reduced matrices of the tuned system from the full tuned system. Follows a detailed explanation on how the same matrices can be computed using only sector level calculations, having as starting point the free interfaces stiffness and mass matrices of the fundamental sector of the tuned system. Eventually it is described how stiffness and density mistuning can be introduced in the final ROMs, what are the hypotheses and approximations necessary for both cases and why it is expected the density mistuning to be a suitable substitution to stiffness mistuning.
- **Chapter 3** compares the results obtained from the analysis performed on the systems described by the ROMs with the results obtained performing the analysis on a FE model of the full system available in Ansys. The model used to apply the methodology is a bladed disk with shrouds at the blades tips and 27 sectors. The comparisons aim to show how the accuracy of the ROMs is impacted by different parameters, such as the size of the ROMs, the kind of mistuning introduced (density or stiffness) and the severity of the mistuning. Moreover, the results cover both the systems in the condition of shroud contact interfaces perfectly clumped (without relative displacement) and the system where the blades are considered cantilever and there is no interaction between the shrouds of two adjacent sectors.
- **Chapter 4** contains the conclusions and final considerations of the theses.

Chapter 2

Methodology

In this section will be discussed in more details how the ROMs of the full system are built, in particular what are approximations introduced and how these affect the final result.

First it will be shown how the reduced matrices of the tuned system can be obtained applying RCCMS to the full tuned system. Then it will be discussed how it is possible to obtain those matrices performing only sector level computations applied to the free interface matrices of the fundamental sector of the tuned system. Eventually it will be shown how mistuning can be directly introduced in the reduced system; both stiffness and density mistuning can be easily introduced, the differences obtained in the two cases will be discussed then in the results section.

2.1 Reduction applied to a full bladed disk's system

In this section it will be showed how the reduction of a full system can operated, the goal is to express clearly all the terms in the final reduced matrices so that, in the following sections, can be studied a way to express those terms operating exclusively at a single sector level.

The equation of motion relative to the Full System is:

$$\left[M_{tot} \right] \left\{ \ddot{X}_{tot} \right\} + \left[K_{tot} \right] \left\{ X_{tot} \right\} = \left\{ 0 \right\} \quad (2.1)$$

It is possible to define:

- **N**: Number of sectors of the bladed disk
- **M**: Number of DOFs per sector

The dimensions of M_{tot} and K_{tot} will be $MN \times MN$.

The matrices are ordered grouping the DOFs of each sector, they will be consistent with this representation of the X_{tot} vector:

$$\{X_{tot}\} = \begin{Bmatrix} X_1 \\ X_2 \\ \vdots \\ X_n \\ \vdots \\ X_N \end{Bmatrix} \quad (2.2)$$

Where every X_n vector is $M \times 1$ and is associated the n -th sector.

The internal ordering of every vector is defined as follows:

$$\{X_n\} = \begin{Bmatrix} X_{sh,H} \\ X_{sh,L} \\ X_{di,H} \\ X_{int} \end{Bmatrix} \quad (2.3)$$

Where:

- $X_{sh,H}$ and $X_{sh,L}$: DOFs relative to the contact interfaces (High and Low) at the shroud, ($L_{sh} \times 1$)
- $X_{di,H}$: DOFs relative to the disk interfaces (High), ($L_{di} \times 1$)
- X_{int} : DOFs relative to the internal nodes of each sector, ($L_{int} \times 1$)

It is clearly true that $2L_{sh} + L_{di} + L_{int} = M$.

In order to proceed in a more convenient way it is better to reorder the matrices, separating the shroud DOFs of each sector from the other DOFs.

The matrices are reordered to be consistent with:

$$\{X_{tot}\} = \begin{Bmatrix} \{X_{sh,H}\} \\ \{X_{sh,L}\} \\ \{X_{di,H}\} \\ \{X_{int}\} \end{Bmatrix} \quad (2.4)$$

Where every partition is defined for example as:

$$\{X_{sh,H}\} = \begin{Bmatrix} \{X_{sh,H}\}_1 \\ \{X_{sh,H}\}_2 \\ \vdots \\ \{X_{sh,H}\}_n \\ \vdots \\ \{X_{sh,H}\}_N \end{Bmatrix} \quad (2.5)$$

To clarify, the dimensions of the partitions are:

- $\{X_{sh,H}\}$ and $\{X_{sh,L}\}$: $NL_{sh} \times 1$
- $\{X_{di,H}\}$: $NL_{di} \times 1$
- $\{X_{int}\}$: $NL_{int} \times 1$

It is useful to introduce relative coordinates between the shroud DOFs of two adjacent sectors, the definition for the generic sector is:

$$\{X_{rel}\}_n = \{X_{sh,L}\}_n - \{X_{sh,H}\}_{n-1} \quad (2.6)$$

It is now possible to have a simple linear transformation that allows to go from the absolute coordinate system to the relative one:

$$\begin{Bmatrix} \begin{Bmatrix} \vdots \\ \{X_{shroud,H}\}_{n-1} \\ \{X_{shroud,H}\}_n \\ \{X_{shroud,H}\}_{n+1} \\ \vdots \\ \{X_{sh,L}\} \\ \{X_{di,H}\} \\ \{X_{int}\} \end{Bmatrix} \\ \vdots \\ \vdots \end{Bmatrix} = [T] \begin{Bmatrix} \begin{Bmatrix} \vdots \\ \{X_{rel}\}_{n-1} \\ \{X_{rel}\}_n \\ \{X_{rel}\}_{n+1} \\ \vdots \\ \{X_{sh,L}\} \\ \{X_{di,H}\} \\ \{X_{int}\} \end{Bmatrix} \\ \vdots \\ \vdots \end{Bmatrix} \quad (2.7)$$

Where $[T]$ is the transformation matrix.

Combining the various reordering and transformation matrices, the full system can now be expressed as:

$$\begin{bmatrix} M_{NN} & M_{NL} \\ M_{LN} & M_{LL} \end{bmatrix} \begin{Bmatrix} \ddot{X}_{rel} \\ \ddot{X}_{slave} \end{Bmatrix} + \begin{bmatrix} K_{NN} & K_{NL} \\ K_{LN} & K_{LL} \end{bmatrix} \begin{Bmatrix} X_{rel} \\ X_{slave} \end{Bmatrix} = \begin{Bmatrix} 0 \\ 0 \end{Bmatrix} \quad (2.8)$$

Where X_{rel} is $NL_{sh} \times 1$ and is composed of all the $\{X_{rel}\}_n$, while X_{slave} is $N(L_{sh} + L_{di} + L_i) \times 1$ and contains everything else.

A constraint mode is defined as the static deformation of the system when a unitary displacement is applied to one relative DOF, to compute all of them, the following equation must be solved:

$$[K_{LL}] \{X_{slave}\} = -[K_{LN}] \{X_{rel}\} \quad (2.9)$$

$$\{X_{slave}\} = -[K_{LL}]^{-1} [K_{LN}] \{X_{rel}\} \quad (2.10)$$

Imposing every time a unitary displacement to one relative DOF and zero to the others can be done using the identity matrix:

$$[\Psi_c] = -[K_{LL}]^{-1} [K_{LN}] [I] \quad (2.11)$$

Given that $[I]$ is $NL_{sh} \times NL_{sh}$, $[\Psi_c]$ will be $N(L_{sh} + L_{di} + L_i) \times N(L_{sh} + L_{di} + L_i)$.

The full matrix with the static modes can be built combining the displacement imposed and the the one calculated:

$$[\Psi] = \begin{bmatrix} [I] \\ [\Psi_c] \end{bmatrix} \quad (2.12)$$

The full size will be $NM \times NL_{sh}$.

The full stick modes are defined as the mode shapes of the system with the shrouds interfaces merged between the sectors. This can be computed by imposing null the relative DOFs defined before, this results in a standard eigenvector problem of the system:

$$[M_{LL}] \{\ddot{X}_{slave}\} + [K_{LL}] \{X_{slave}\} = \{0\} \quad (2.13)$$

Given that $[\Phi_i]$ are the eigenvectors of this system, the complete mode shapes can be again obtained by considering the partition given by the DOFs imposed and the one calculated:

$$[\Phi] = \begin{bmatrix} [0] \\ [\Phi_i] \end{bmatrix} \quad (2.14)$$

The complete set of eigenvectors is $NM \times N(L_{sh} + L_{di} + L_i)$, but it can be reduced by retaining a reduced number of vectors and would become $NM \times ret_mode$, where $ret_mode \ll N(L_{sh} + L_{di} + L_i)$ is the number of eigenvectors retained.

We can now define the transformation:

$$\begin{Bmatrix} X_{rel} \\ X_{slave} \end{Bmatrix} = \begin{bmatrix} [I] & [0] \\ [\Psi_c] & [\Phi_i] \end{bmatrix} \begin{Bmatrix} X_{rel} \\ X_{gen} \end{Bmatrix} \quad (2.15)$$

Where X_{gen} is a set of generalized coordinates, considering the reduced set of full stick modes, will be $ret_mode \times 1$. Performing the change of coordinates will result in:

$$\begin{aligned} & \begin{bmatrix} M_{NN} & M_{NL} \\ M_{LN} & M_{LL} \end{bmatrix} \begin{bmatrix} [I] & [0] \\ [\Psi_c] & [\Phi_i] \end{bmatrix} \begin{Bmatrix} \ddot{X}_{rel} \\ \ddot{X}_{gen} \end{Bmatrix} + \\ & + \begin{bmatrix} K_{NN} & K_{NL} \\ K_{LN} & K_{LL} \end{bmatrix} \begin{bmatrix} [I] & [0] \\ [\Psi_c] & [\Phi_i] \end{bmatrix} \begin{Bmatrix} X_{rel} \\ X_{gen} \end{Bmatrix} = \begin{Bmatrix} 0 \\ 0 \end{Bmatrix} \end{aligned} \quad (2.16)$$

To balance the equation it is necessary to multiply the reduction matrix on the left side of the equation as well:

$$\begin{aligned} & \begin{bmatrix} [I] & [0] \\ [\Psi_c] & [\Phi_i] \end{bmatrix}^T \begin{bmatrix} M_{NN} & M_{NL} \\ M_{LN} & M_{LL} \end{bmatrix} \begin{bmatrix} [I] & [0] \\ [\Psi_c] & [\Phi_i] \end{bmatrix} \begin{Bmatrix} \ddot{X}_{rel} \\ \ddot{X}_{gen} \end{Bmatrix} + \\ & + \begin{bmatrix} [I] & [0] \\ [\Psi_c] & [\Phi_i] \end{bmatrix}^T \begin{bmatrix} K_{NN} & K_{NL} \\ K_{LN} & K_{LL} \end{bmatrix} \begin{bmatrix} [I] & [0] \\ [\Psi_c] & [\Phi_i] \end{bmatrix} \begin{Bmatrix} X_{rel} \\ X_{gen} \end{Bmatrix} = \begin{Bmatrix} 0 \\ 0 \end{Bmatrix} \end{aligned} \quad (2.17)$$

Performing the multiplication, the result is:

$$\begin{bmatrix} M_{Guyan} & M_{rg} \\ M_{rg}^T & M_{id} \end{bmatrix} \begin{Bmatrix} \ddot{X}_{rel} \\ \ddot{X}_{gen} \end{Bmatrix} + \begin{bmatrix} K_{Guyan} & K_{rg} \\ K_{rg}^T & K_{\Lambda} \end{bmatrix} \begin{Bmatrix} X_{rel} \\ X_{gen} \end{Bmatrix} = \begin{Bmatrix} 0 \\ 0 \end{Bmatrix} \quad (2.18)$$

Where the partition of the mass matrix are:

$$\begin{cases} M_{Guyan} = M_{NN} + \Psi_c^T M_{LN} + M_{NL} \Psi_c + \Psi_c^T M_{LL} \Psi_c \\ M_{rg} = M_{NL} \Phi_i + \Psi_c^T M_{LL} \Phi_i \\ M_{id} = \Phi_i^T M_{LL} \Phi_i = I \end{cases} \quad (2.19)$$

The partition of the stiffness matrix are:

$$\begin{cases} K_{Guyan} = K_{NN} + \Psi_c^T K_{LN} + K_{NL} \Psi_c + \Psi_c^T K_{LL} \Psi_c \\ K_{rg} = K_{NL} \Phi_i + \Psi_c^T K_{LL} \Phi_i \\ K_{\Lambda} = \Phi_i^T K_{LL} \Phi_i \end{cases} \quad (2.20)$$

For the stiffness matrix is possible to simplify the equations by considering that $[\Psi_c] = -[K_{LL}]^{-1}[K_{LN}]$, the Guyan partition becomes:

$$\begin{aligned} K_{Guyan} &= K_{NN} - \left(K_{LL}^{-1}K_{LN}\right)^T K_{LN} - K_{NL} \left(K_{LL}^{-1}K_{LN}\right) + \\ &+ \left(K_{LL}^{-1}K_{LN}\right)^T K_{LL} \left(K_{LL}^{-1}K_{LN}\right) \end{aligned} \quad (2.21)$$

$$K_{Guyan} = K_{NN} - K_{NL}K_{LL}^{-1T}K_{LN} - K_{NL}K_{LL}^{-1}K_{LN} + K_{NL}K_{LL}^{-1T}K_{LL}K_{LL}^{-1}K_{LN} \quad (2.22)$$

$$K_{Guyan} = K_{NN} - K_{NL}K_{LL}^{-1T}K_{LN} \quad (2.23)$$

$$K_{Guyan} = K_{NN} - K_{NL}K_{LL}^{-1}K_{LN} \quad (2.24)$$

The out of diagonal partition becomes:

$$K_{rg} = K_{NL}\Phi_i - \left(K_{LL}^{-1}K_{LN}\right)^T K_{LL}\Phi_i \quad (2.25)$$

$$K_{rg} = K_{NL}\Phi_i - K_{NL}K_{LL}^{-1T}K_{LL}\Phi_i \quad (2.26)$$

$$K_{rg} = 0 \quad (2.27)$$

Eventually what is left is:

$$\begin{bmatrix} M_{Guyan} & M_{rg} \\ M_{rg}^T & M_{id} \end{bmatrix} \begin{Bmatrix} \ddot{X}_{rel} \\ \ddot{X}_{gen} \end{Bmatrix} + \begin{bmatrix} K_{Guyan} & 0 \\ 0 & K_{\Lambda} \end{bmatrix} \begin{Bmatrix} X_{rel} \\ X_{gen} \end{Bmatrix} = \begin{Bmatrix} 0 \\ 0 \end{Bmatrix} \quad (2.28)$$

2.2 Sector level calculations

Given that equation 2.17 can be expressed as:

$$\begin{bmatrix} [\Psi]^T \\ [\Phi]^T \end{bmatrix} [M_{tot}] \begin{bmatrix} [\Psi] & [\Phi] \end{bmatrix} \begin{Bmatrix} \ddot{X}_{rel} \\ \ddot{X}_{gen} \end{Bmatrix} + \begin{bmatrix} [\Psi]^T \\ [\Phi]^T \end{bmatrix} [K_{tot}] \begin{bmatrix} [\Psi] & [\Phi] \end{bmatrix} \begin{Bmatrix} X_{rel} \\ X_{gen} \end{Bmatrix} = \begin{Bmatrix} 0 \\ 0 \end{Bmatrix} \quad (2.29)$$

Performing the matrices multiplications:

$$\begin{bmatrix} \Psi^T M_{tot} \Psi & \Psi^T M_{tot} \Phi \\ \Phi^T M_{tot} \Psi & \Phi^T M_{tot} \Phi \end{bmatrix} \begin{Bmatrix} \ddot{X}_{rel} \\ \ddot{X}_{gen} \end{Bmatrix} + \begin{bmatrix} \Psi^T K_{tot} \Psi & \Psi^T K_{tot} \Phi \\ \Phi^T K_{tot} \Psi & \Phi^T K_{tot} \Phi \end{bmatrix} \begin{Bmatrix} X_{rel} \\ X_{gen} \end{Bmatrix} = \begin{Bmatrix} 0 \\ 0 \end{Bmatrix} \quad (2.30)$$

Comparing this equation with equation 2.28, it is possible to define the different partitions in an alternative way:

$$\begin{cases} M_{Guyan} = \Psi^T M_{tot} \Psi \\ M_{rg} = \Psi^T M_{tot} \Phi \\ M_{id} = \Phi^T M_{tot} \Phi \end{cases} \quad (2.31)$$

$$\begin{cases} K_{Guyan} = \Psi^T K_{tot} \Psi \\ K_{\Lambda} = \Phi^T K_{tot} \Phi \end{cases} \quad (2.32)$$

Considering that, accordingly with the theory of finite elements, the matrices of the full system are built as a summation of the contribution of the single sectors, we can express:

$$[M_{tot}] = \sum_{n=1}^N [M^0] \quad (2.33)$$

$$[K_{tot}] = \sum_{n=1}^N [K^0] \quad (2.34)$$

Where the $[M^0]$ and $[K^0]$ matrices are the free-interfaces matrices of the sector. For more details on how the summation is performed see [2].

After this consideration it is possible to perform the substitution and obtain:

$$\begin{cases} M_{Guyan} = \Psi^T \left(\sum_{n=1}^N [M^0] \right) \Psi \\ M_{rg} = \Psi^T \left(\sum_{n=1}^N [M^0] \right) \Phi \\ M_{id} = \Phi^T \left(\sum_{n=1}^N [M^0] \right) \Phi \end{cases} \quad (2.35)$$

$$\begin{cases} K_{Guyan} = \Psi^T \left(\sum_{n=1}^N [K^0] \right) \Psi \\ K_{\Lambda} = \Phi^T \left(\sum_{n=1}^N [K^0] \right) \Phi \end{cases} \quad (2.36)$$

It is possible to further modify the equations and express the products of this matrices (full system level size) as the summation of the products of smaller matrices (sector level size):

$$\begin{cases} M_{Guyan} = \sum_{n=1}^N \Psi_{f,n}^T [M^0] \Psi_{f,n} \\ M_{rg} = \sum_{n=1}^N \Psi_{f,n}^T [M^0] \Phi_{f,n} \\ M_{id} = \sum_{n=1}^N \Phi_{f,n}^T [M^0] \Phi_{f,n} \end{cases} \quad (2.37)$$

$$\begin{cases} K_{Guyan} = \sum_{n=1}^N \Psi_{f,n}^T [K^0] \Psi_{f,n} \\ K_{\Lambda} = \sum_{n=1}^N \Phi_{f,n}^T [K^0] \Phi_{f,n} \end{cases} \quad (2.38)$$

Where $\Psi_{f,n}$ and $\Phi_{f,n}$ are the f rows of the modes matrices corresponding to the $n - th$ sector.

All the elements now in the equations are obtainable from sector level calculations, without having to work with the matrices of the full system.

It is important to make sure that all the partitions are computed using all the matrices expressed in a consistent set of coordinates. In this case, since it will be assumed that $[M^0]$ and $[K^0]$ will be given in absolute physical coordinates, all the modes will be computed in a efficient set of coordinates and then expressed in the absolute-physical set.

2.3 Full stick modes

In this section will be discussed how it is possible to compute the full stick modes of the full system.

The starting point of the implementation will be the mass and stiffness matrices of a sector of a bladed disk obtained from a FEM software.

From the FEM software it is also obtained a mapping file that allows to understand which line and columns of the matrices are referring to which DOFs. The entirety of the DOFs will then be divided in the same smaller groups that have already been considered in the previous sections. In particular it is possible to distinguish the disk interfaces nodes, the shroud interfaces nodes and the internal nodes, which are all the nodes not contained in the previous groups.

The matrices are reordered to be consistent with a displacement vector defined as follows:

$$\{X\} = \begin{Bmatrix} X_{sh,H} \\ X_{sh,L} \\ X_{di,H} \\ X_{di,L} \\ X_{int} \end{Bmatrix} \quad (2.39)$$

During the reduction process will be exploited in different ways the cyclic symmetry of the full system, so it is useful to define the inter-blade phase angle:

$$\varphi = h \frac{2\pi}{N} \quad (2.40)$$

Where N is the number of sectors in the full system and h is the harmonic index.

It is possible to define a linear transformation to go from the physical coordinates sets of the system obtained from the FEM software to an equivalent set of

coordinates that assumes the repetition of N sectors in the disk.

The transformation matrix is defined as:

$$[C] = \begin{bmatrix} I & 0 & 0 & 0 \\ 0 & I & 0 & 0 \\ 0 & 0 & I & 0 \\ 0 & 0 & Ie^{-i\varphi} & 0 \\ 0 & 0 & 0 & I \end{bmatrix} \quad (2.41)$$

Where the I and 0 are, in fact, identity and zeros matrices of the correct dimension to perform the following multiplication:

$$\begin{Bmatrix} X_{sh,H} \\ X_{sh,L} \\ X_{di,H} \\ X_{di,L} \\ X_{int} \end{Bmatrix} = [C] \begin{Bmatrix} X_{sh,H} \\ X_{sh,L} \\ X_{di,H} \\ X_{int} \end{Bmatrix}_{cyc} \quad (2.42)$$

Furthermore it is possible to define a transformation matrix to introduce relative coordinates between the shroud interfaces of two adjacent sectors. Before that it is convenient to clarify that, since it is possible to correlate the corresponding nodes of two sectors taking into account the cyclic symmetry of the full system, it is true that:

$$\{X_{sh,H}\}_{n-1} = \{X_{sh,H}\}_n e^{-i\varphi} \quad (2.43)$$

The definition of the relative coordinates that are going to be used is the one in equation 2.6:

$$\{X_{rel}\}_n = \{X_{sh,L}\}_n - \{X_{sh,H}\}_{n-1} \quad (2.44)$$

And so:

$$\{X_{rel}\}_n = \{X_{sh,L}\}_n - \{X_{sh,H}\}_n e^{-i\varphi} \quad (2.45)$$

The transformation matrix is then:

$$[V] = \begin{bmatrix} -Ie^{i\varphi} & Ie^{i\varphi} & 0 & 0 \\ 0 & I & 0 & 0 \\ 0 & 0 & I & 0 \\ 0 & 0 & 0 & I \end{bmatrix} \quad (2.46)$$

And it is then valid the equation:

$$\begin{Bmatrix} X_{sh,H} \\ X_{sh,L} \\ X_{di,H} \\ X_{int} \end{Bmatrix}_{cyc} = [V] \begin{Bmatrix} X_{rel} \\ X_{sh,L} \\ X_{di,H} \\ X_{int} \end{Bmatrix}_{rel,cyc} \quad (2.47)$$

It is now possible to operate all the substitutions introduced in the equation of motion of the single sector:

$$[M^0] \{\ddot{X}\} + [K^0] \{X\} = \{0\} \quad (2.48)$$

$$[M^0] [C] \{\ddot{X}\}_{cyc} + [K^0] [C] \{X\}_{cyc} = \{0\} \quad (2.49)$$

$$[M^0] [C] [V] \{\ddot{X}\}_{rel,cyc} + [K^0] [C] [V] \{X\}_{rel,cyc} = \{0\} \quad (2.50)$$

The equation is then balanced:

$$[V]^T [C]^T [M^0] [C] [V] \{\ddot{X}\}_{rel,cyc} + [V]^T [C]^T [K^0] [C] [V] \{X\}_{rel,cyc} = \{0\} \quad (2.51)$$

Consistently with the notation of the displacement vector, it is possible to define the matrices:

$$\begin{cases} [M^0]_{rel,cyc} = [V]^T [C]^T [M^0] [C] [V] \\ [K^0]_{rel,cyc} = [V]^T [C]^T [K^0] [C] [V] \end{cases} \quad (2.52)$$

The size of this matrices has to be consistent with the displacement vector, and so they are $2L_{sh} + L_{di} + L_{int} \times 2L_{sh} + L_{di} + L_{int}$.

The equation is rewritten as:

$$[M^0]_{rel,cyc} \{\ddot{X}_s\}_{rel,cyc} + [K^0]_{rel,cyc} \{X_s\}_{rel,cyc} = \{0\} \quad (2.53)$$

The full stick modes of a single sector (once the harmonic index is defined) are obtainable by solving the eigenvalues/eigenvectors problem of the system defined by the $[M^0]_{rel,cyc}$ and $[K^0]_{rel,cyc}$ matrices, after having imposed null the relative displacement.

The result of the solution of the eigenvector problem is a matrix of p columns (where p is the number of eigenvector we decided to compute), each one representing one eigenvector. The mode shapes obtained are consistent with the matrix ordering considered in the problem, so the generic column of the full stick modes matrix is:

$$\{\Phi\}_c = \begin{Bmatrix} \Phi_{sh,L} \\ \Phi_{di,H} \\ \Phi_{int} \end{Bmatrix} \quad (2.54)$$

It is useful to modify the mode shapes so that they have all the partitions present in the equation 2.39.

Considering the cyclic symmetry, it is possible to obtain the high shroud interface DOFs from the low one. This is possible because for the full stick modes it has been imposed that the relative displacement of the shroud interfaces of two adjacent sectors is zero:

$$\{X_{sh,L}\}_n - \{X_{sh,H}\}_{n-1} = \{0\} \quad (2.55)$$

$$\{X_{sh,L}\}_n - \{X_{sh,H}\}_n e^{-i\varphi} = \{0\} \quad (2.56)$$

$$\{X_{sh,H}\}_n = \{X_{sh,L}\}_n e^{i\varphi} \quad (2.57)$$

Considering the cyclic symmetry of the system is also possible to express the partition of the low disk interface as function of the high one.

With this considerations it is possible to define another version of the full stick modes:

$$\{\Phi\}_s = \begin{Bmatrix} \Phi_{sh,L} e^{i\varphi} \\ \Phi_{sh,L} \\ \Phi_{di,H} \\ \Phi_{di,H} e^{-i\varphi} \\ \Phi_{int} \end{Bmatrix} \quad (2.58)$$

To build the full disk mode shape, it is possible to either consider the cyclic symmetry and the relation available for two adjacent sectors: $\{\Phi\}_{s,n+1} = \{\Phi\}_{s,n} e^{ih \frac{2\pi}{N}}$.

$$\{\Phi\} = \begin{Bmatrix} \{\Phi\}_{s,1} \\ \{\Phi\}_{s,1} e^{i\varphi} \\ \vdots \\ \{\Phi\}_{s,1} e^{i(n-1)\varphi} \\ \vdots \\ \{\Phi\}_{s,1} e^{i(N-1)\varphi} \end{Bmatrix} \quad (2.59)$$

Or, since this operation has to be done considering the different harmonic indices, it is possible to take advantage of the property of the discrete Fourier matrix. It is possible to build the final matrix of the full system mode shapes as:

$$[\Phi] = (E_N \otimes I_{M+L_{sh}}) Bdiag [\Phi_{s,h}] \quad (2.60)$$

Where $Bdiag [\Phi_{s,h}]$ is a block diagonal matrix composed with the p $\{\Phi\}_s$ mode shapes of every harmonic index. E_N is the discrete Fourier matrix of size $N \times N$,

whose elements are defined as:

$$(E_N)_{j,k} = \frac{1}{\sqrt{N}} e^{i\frac{2\pi}{N}(j-1)(k-1)} \quad (2.61)$$

For a more complete description of the discrete Fourier matrices or the Kronecker products see [3].

To better explain this procedure let's consider a simplified example. Let's consider just a 4×4 Fourier matrix and only DOF per sector, so that it is not necessary to scale with the Kronecker product.

The Fourier matrix will be:

$$E_4 = \frac{1}{2} \begin{bmatrix} 1 & 1 & 1 & 1 \\ 1 & i & -1 & -i \\ 1 & -1 & 1 & -1 \\ 1 & -i & -1 & i \end{bmatrix} \quad (2.62)$$

The full stick modes matrix will be:

$$Bdiag[\Phi_{s,h}] = \begin{bmatrix} \Phi_{s,h=0} & 0 & 0 & 0 \\ 0 & \Phi_{s,h=1} & 0 & 0 \\ 0 & 0 & \Phi_{s,h=2} & 0 \\ 0 & 0 & 0 & \Phi_{s,h=3} \end{bmatrix} \quad (2.63)$$

Performing the multiplication the result will be:

$$[\Phi] = \frac{1}{2} \begin{bmatrix} 1 & 1 & 1 & 1 \\ 1 & i & -1 & -i \\ 1 & -1 & 1 & -1 \\ 1 & -i & -1 & i \end{bmatrix} \begin{bmatrix} \Phi_{s,h=0} & 0 & 0 & 0 \\ 0 & \Phi_{s,h=1} & 0 & 0 \\ 0 & 0 & \Phi_{s,h=2} & 0 \\ 0 & 0 & 0 & \Phi_{s,h=3} \end{bmatrix} \quad (2.64)$$

$$[\Phi] = \frac{1}{2} \begin{bmatrix} \Phi_{s,h=0} & \Phi_{s,h=1} & \Phi_{s,h=2} & \Phi_{s,h=3} \\ \Phi_{s,h=0} & i\Phi_{s,h=1} & -\Phi_{s,h=2} & -i\Phi_{s,h=3} \\ \Phi_{s,h=0} & -\Phi_{s,h=1} & \Phi_{s,h=2} & -\Phi_{s,h=3} \\ \Phi_{s,h=0} & -i\Phi_{s,h=1} & -\Phi_{s,h=2} & i\Phi_{s,h=3} \end{bmatrix} \quad (2.65)$$

It is shown how every mode is rotated, according to his own harmonic index, on the column of the resulting matrix. It is also possible to notice that the modes do not interact with each other, and every element of the final matrix is just a rotation of a initially computed mode. With more than one DOF per sector, The Kronecker product assures that the dimensions of the multiplication agree, but the concept remains the same.

Either way it is now available the matrix of the full stick modes of dimensions $N(2L_{sh} + 2L_{di} + L_{int}) \times N(2L_{sh} + 2L_{di} + L_{int})$ where the columns are a sequence of $\{\Phi\}_s$ vectors whose dimensions and organization are consistent with the $[M^0]$ and $[K^0]$ matrices.

2.4 Constraint modes

As for the full stick modes, the computation of the constraint modes must be done having available only the free-interfaces matrices of the generic sector.

This operation can be done performing a change of coordinates on the static problem considered in equation 2.9:

$$\begin{cases} \{X_{slave}\} = [E_N \otimes I_{L_{sh}+L_{di}+L_{int}}] \{X_{slave}\}_{cyc} \\ \{X_{rel}\} = [E_N \otimes I_{L_{sh}}] \{X_{rel}\}_{cyc} \end{cases} \quad (2.66)$$

Performing the substitution and the balancing in the static problem results in a decoupling of the equations due to the results of the application of the Fourier matrices to the block circulant matrix $[K_{LL}]$ (for more details see the appendices of [4]).

It is then possible to solve multiple static problems (one per harmonic index) at a sector level and obtain portions of the constraint modes.

Given that the final constraint modes will have the following structure:

$$\{\Psi_{slave}\}_{cyc} = \begin{pmatrix} \{\Psi_{slave}\}_{cyc,0} \\ \{\Psi_{slave}\}_{cyc,1} \\ \vdots \\ \{\Psi_{slave}\}_{cyc,N-1} \end{pmatrix} \quad (2.67)$$

Each portion can be computed as:

$$\{\Psi_{slave}\}_{cyc,n} = -[K_{LL}^0]^{-1}[K_{LN}^0]\{\Psi_{rel}\}_{cyc,n} \quad (2.68)$$

Where $[K_{LL}^0]$ and $[K_{LN}^0]$ are the partition of the matrix $[K^0]_{rel,cyc}$ defined for the full stick modes computation.

It is now necessary to express the imposed displacement vector $\{\Psi_{rel}\}_{cyc,n}$, remembering that in physical coordinates it was the identity matrix. First it is possible to reduce the problem since it is only necessary to compute the constraint

modes due to the displacement of all the relative DOFs of one sector; after that it is possible to rotate this modes to obtain the ones resulting from the displacement of the relative DOFs of the other sectors (thanks to the symmetry of the system). So instead of the full identity matrix the imposed unitary displacement $\{\Psi_{rel}\}$ (in physical coordinates) will just be the first L_{sh} columns of the identity matrix $NL_{sh} \times NL_{sh}$.

To obtain the equivalent matrix in cyclic coordinates it is used the inverse of the transformation defined in 2.66:

$$\{\Psi_{rel}\}_{cyc} = [E_N \otimes I_{L_{sh}}]^T \{\Psi_{rel}\} \quad (2.69)$$

Now all the portions of the constraint mode vector can be computed by solving the static problem in cyclic coordinates, using the partitions of the free-interface stiffness matrix (with imposed cyclic boundary conditions and relative coordinates transformation).

Once all the partitions are computed and assembled, it is possible to transform back the constraint modes in physical coordinates using the definition of the transformation:

$$\begin{Bmatrix} \{\Psi_{slave}\}_0 \\ \{\Psi_{slave}\}_1 \\ \vdots \\ \{\Psi_{slave}\}_{N-1} \end{Bmatrix} = [E_N \otimes I_{L_{sh}+L_{di}+L_i}] \{X_{slave}\}_{cyc} \quad (2.70)$$

Where every portion is referred to the same DOFs of different sectors:

$$\{\Psi_{slave}\}_n = \begin{Bmatrix} \{\Psi_{sh,L}\} \\ \{\Psi_{di,H}\} \\ \{\Psi_{int}\} \end{Bmatrix}_n \quad (2.71)$$

Similarly to what has been done for the full stick modes, also for the constraint modes it is useful to express them consistently with the structure of the vector in equation 2.39 and so with the $[M^0]$ and $[K^0]$ matrices.

From equation 2.6, we can express:

$$\{\Psi_{sh,H}\}_n = \{\Psi_{sh,L}\}_{n+1} - \{\Psi_{rel}\}_{n+1} \quad (2.72)$$

And from the consideration made about the cyclic symmetry, we can express:

$$\{\Psi_{di,L}\}_n = \{\Psi_{di,H}\}_{n-1} \quad (2.73)$$

2.5 Reduced matrix computation review

In the first part of this chapter it has been shown how the reduction of a full system with RCCMS affect the matrices of that system, arriving at the expression of equation 2.28 and then it has been shown that the partition in that equation can be expressed in term of summations of sector level terms.

The focus was then on how to actually compute the terms in the summations, having available only the free interfaces matrices of a sector $[M^0]$ and $[K^0]$.

The full stick mode shapes can be computed exploiting the cyclic symmetry of the system to impose the boundary condition on one sector and then it is a eigenvector/eigenvalue problem.

The constraint modes can be computed using the properties of the discrete Fourier matrices, particularly the fact that when they are applied to a block circulant matrix transforming it into a block diagonal matrix. With that it is possible to define N static problems, one per harmonic index, which once solved give portion of the constraint modes. It was then possible to reassemble all the portions and to obtain the final matrix.

2.6 Mistuning introduction

In this section will be shown how mistuning can be directly introduced in the reduced matrices of the full system. The power of this reduction process is shown here, since the introduction of mistuning does not require to recompute neither the constraint modes or the full stick modes with a significant benefit in terms of computing time. Mistuning analysis are usually statistical, that means that are generated many mistuning patterns for a fixed deviation value, having the possibility to generate ROMs for every pattern with close to none additional time required is fundamental.

2.6.1 Stiffness mistuning

First of all is useful to understand how the stiffness mistuning impacts the system. Having a deviation in the stiffness of each sector means that all the $[K^0]$ are different, moreover the full stick modes are different from the tuned case and also the constraint modes change. It is not applicable to compute the mode shapes of the full system for every mistuning pattern, so it is still required to express the reduced matrices with sector level terms.

It is possible to express the stiffness matrix partitions of equation 2.38, taking into account the effect of mistuning:

$$\begin{cases} K_{Guyan}^* = \sum_{n=1}^N \Psi_{f,n}^{*T} [K^0]_n^* \Psi_{f,n}^* \\ K_{\Lambda}^* = \sum_{n=1}^N \Phi_{f,n}^{*T} [K^0]_n^* \Phi_{f,n}^* \end{cases} \quad (2.74)$$

Using the superscript $*$ to specify that the terms are referred to the mistuned system.

The following considerations are introduced in further details in [1], fourth chapter.

Introducing the hypotheses of cyclic static modes which states that the effect of mistuning negligible on the constraint modes allows to use the same constraint modes already computed for the tuned case.

Introducing the hypotheses of small mistuning which states that the mode shapes of the mistuned system can be expressed as a linear combination of the ones of the tuned system allows to express the mistuned full stick modes as:

$$[\Phi_f]_n^* = [\Phi_f]_n [P] \quad (2.75)$$

Where $[P]$ is the coefficient matrix of the transformation, performing the substitution in the expression above allows to use the full stick modes of the tuned systems and apply $[P]$ to the generalized coordinates partition of the displacement vector.

Last it is possible to express the mistuned stiffness matrix of the single sector as:

$$[K^0]_n^* = [K^0]_n + [\Delta K^0]_n \quad (2.76)$$

Where $[\Delta K^0]_n$ is the effect of the mistuning on the stiffness matrix of one specific sector.

The mistuning has usually been introduced in term of a pattern of small deviations of the sectors stiffness.

The deviation of the stiffness introduced for every sector is defined as:

$$\delta_n = \frac{E_{mist,n}}{E_{mat}} \quad (2.77)$$

Where E_{mat} is the Young modulus of the material in tuned conditions, while $E_{mist,n}$ is the Young modulus of the material considered the mistuning of that sector.

It is possible then to express the stiffness matrix of every mistuned sector as:

$$[K^0]_n^* = \delta_n [K^0] \quad (2.78)$$

With all this considerations the introduction of the stiffness mistuning can be performed as follows:

$$\begin{cases} K_{Guyan}^* = \sum_{n=1}^N \delta_n \Psi_{f,n}^T [K^0] \Psi_{f,n} \\ K_{\Lambda}^* = \sum_{n=1}^N \delta_n \Phi_{f,n}^T [K^0] \Phi_{f,n} \end{cases} \quad (2.79)$$

The out of diagonal partitions of the stiffness matrix, which in the tuned case are all zeros, are expected to be close to null even in the mistuned case and so they are neglected.

It is immediate to see how the building process of the reduced matrices can stay the same as the tuned case until the very final assembling. There is no need to compute again the static or constraint modes.

2.6.2 Density mistuning

The introduction of density mistuning can be done following the same steps of the stiffness mistuning, but some differences must be taken into account. Without any hypotheses introduced, it is assumed, as was for the stiffness mistuning, that all the terms in 2.37 are different in the mistuned case from the tuned case:

$$\begin{cases} M_{Guyan}^* = \sum_{n=1}^N \Psi_{f,n}^{*T} [M^0]_n^* \Psi_{f,n}^* \\ M_{rg}^* = \sum_{n=1}^N \Psi_{f,n}^{*T} [M^0]_n^* \Phi_{f,n}^* \\ M_{id}^* = \sum_{n=1}^N \Phi_{f,n}^{*T} [M^0]_n^* \Phi_{f,n}^* \end{cases} \quad (2.80)$$

Here it is possible to see where the introduction of the mistuning in terms of density deviations is powerful. Since, in this case, the stiffness matrix is exact, then the constraint modes of the mistuned system are the same of the the tuned system. This can be understood considering the definition of constraint modes, equation 2.9. In fact physically these modes are static deformations, which do not depend in any way from the mass of the system.

The rest of the considerations are the same as for the stiffness mistuning. Under the hypotheses of small mistuning the full stick modes of the mistuned system can

be seen as a linear combination of the full stick modes of the tuned system. While the mass matrices of the mistuned system can again be decomposed in their tuned counterparts and a deviation due to the presence of the mistuning:

$$[M^0]_n^* = [M^0] + [\Delta M^0]_n \quad (2.81)$$

In this case the deviation parameter is defined as:

$$\delta_n = \frac{\rho_{mist,n}}{\rho_{mat}} \quad (2.82)$$

Where ρ_{mat} is the density of the material in tuned conditions, while $\rho_{mist,n}$ is the density of the material considered the mistuning of that sector.

The mass matrix of the mistuned sector can be then expressed as:

$$[M^0]_n^* = \delta_n [M^0] \quad (2.83)$$

Eventually, the partitions of the mistuned reduced mass matrix can be expressed as:

$$\left\{ \begin{array}{l} M_{Guyan}^* = \sum_{n=1}^N \delta_n \Psi_{f,n}^T [M^0]_n \Psi_{f,n} \\ M_{rg}^* = \sum_{n=1}^N \delta_n \Psi_{f,n}^T [M^0]_n \Phi_{f,n} \\ M_{id}^* = \sum_{n=1}^N \delta_n \Phi_{f,n}^T [M^0]_n \Phi_{f,n} \end{array} \right. \quad (2.84)$$

In this case as well are still valid all the considerations made for the stiffness mistuning and also it worth mentioning again how this time was not introduced the hypotheses of cyclic static modes, which brings a reduction of the accuracy of the ROM, but it is mandatory for the stiffness mistuning case since it was imposed as a requirement to be able to express all the terms in the matrices performing only sector level calculations.

Chapter 3

Results

In this chapter the results obtained will be presented in terms of natural frequencies, mode shapes and linear forced response. The comparison will be between the analysis performed on the system described by the reduced matrices built following the methodology described in the previous chapter, with the analysis performed on the full model of the bladed disk, available in Ansys.

3.1 Description of the models

3.1.1 FE model

The model considered in this thesis is a simplified model of a bladed disk with 27 sectors, composed of 449226 degrees of freedom (149742 nodes). The single sector model (considering both disk interfaces) has 17484 DOFs (5828 nodes).

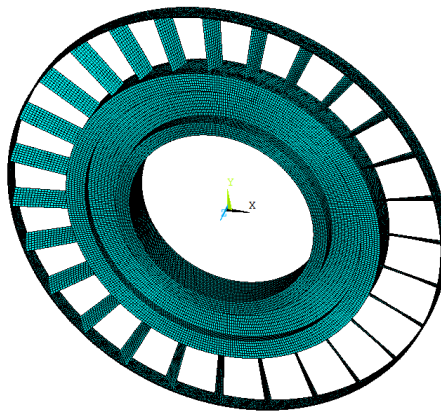


Figure 3.1: Full bladed disk

In this case, it is possible to identify the partitions of the fundamental sector described in the methodology chapter:

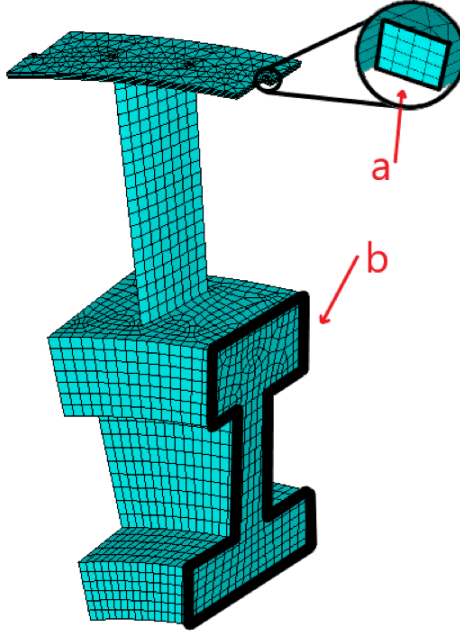


Figure 3.2: Elemental sector, (a) Shroud interface, (b) Disk interface

The low and high interfaces have the same number of DOFs, the shroud interfaces have $L_{sh} = 75$ DOFs, the disk interfaces have $L_{di} = 846$ DOFs there are then $L_{int} = 15642$ internal DOFs. The FEM model has also additional DOFs on which are imposed the constraints, these DOFs are not counted in the list, since imposing there no displacement at all is equivalent at excluding those DOFs from mass and stiffness matrices of the system.

The mistuning will be introduced in the FEM model changing the characteristics of the material sector by sector. It has also been considered the case in which the mistuning is introduced only on the blades DOFs, while the disk is not affected by it. This cases were introduced to test the performances of the ROMs with a simplified case compared to the full sector mistuning described earlier.

3.1.2 Reduced order models

The reduced order models used in the following sections will be defined by their size, usually bigger ROMs better approximate the real system, and the characteristics

of the mistuning introduced.

The size of the ROM will be defined by the number of full stick modes that are retained during the reduction process. In this case the choice is to retain a equal amount of modes for every harmonic index, the cases considered will be with 5, 10, 20 and 30 modes per nodal diameter (ND) which results in reduced matrices with, respectively, 2160, 2295, 2565 and 2835 rows and columns.

3.1.3 Mistuning patterns

The system is strongly impacted by the mistuning pattern and since the objective of this theses is to compare the performance of the ROMs when introducing different types of mistuning, it is necessary to be able to have stiffness and density mistuning patterns that have similar impact on the system. This is accomplished by generating patterns of δ_n that can be introduced in equations 2.79 and 2.84 into the ROMs and can be used to define the material properties of the sectors of the FE models.

Let's define δ_{stiff} the vector of δ_n applied in the stiffness mistuning case and δ_{dens} the vector of δ_n applied in the density mistuning case. Clearly having the same pattern introduced for both would not result in similar systems since, in general, stiffness and density contribute to the dynamic of the system as one the inverse of the other. But defining $\delta_{dens} = \delta_{stiff}^{-1}$ is not possible as well, because for small mistuning it is valid the hypotheses that, in the real bladed disks, the imperfection causing the mistuning do not impact the overall stiffness or density of the components. This is verified in the reduced order models if the averages of the δ vectors are unitary. So, if δ_{dens} is a function of δ_{stiff} and the stiffness mistuning pattern is defined to have average 1, the transformation function must be linear to assure that also the density mistuning pattern has also average 1.

Always under the hypotheses of small mistuning it is possible to consider the Taylor expansion valid for values really close to 1 of the function introduced before, so that the transformation is linear:

$$\delta_{stiff} = \delta_{dens}^{-1} \simeq 2 - \delta_{dens} \quad (3.1)$$

This transformation is not supposed to make sure that the two generated systems are the exact same, its porpoise is to only to assure that the systems are similar enough so that the difference in performances of the ROMs generated to approximate them are not dependent on the mistuning patterns, but only on type of

mistuning. The validity of this assumption is assessed in the appendix A.

The stiffness mistuning patterns introduced will be sampled from normal distributions with different standard deviation, 3% and 6%. Then the average will be set to 1 and the density mistuning patterns will be generated using equation 3.1:

δ_{stiff} 3%	δ_{dens} 3%	δ_{stiff} 6%	δ_{dens} 6%
0.971	1.029	0.941	1.059
0.978	1.022	0.957	1.043
1.006	0.994	1.012	0.988
0.989	1.011	0.978	1.022
1.000	1.000	1.000	1.000
1.014	0.986	1.029	0.971
1.008	0.992	1.016	0.984
1.017	0.983	1.034	0.966
1.012	0.988	1.024	0.976
0.998	1.002	0.996	1.004
1.008	0.992	1.016	0.984
1.003	0.997	1.006	0.994
1.011	0.989	1.022	0.978
1.007	0.993	1.013	0.987
1.007	0.993	1.014	0.986
0.991	1.009	0.982	1.018
0.998	1.002	0.996	1.004
0.975	1.025	0.950	1.050
1.004	0.996	1.007	0.993
0.998	1.002	0.996	1.004
0.999	1.001	0.999	1.001
1.012	0.988	1.024	0.976
0.992	1.008	0.985	1.015
0.974	1.026	0.948	1.052
0.992	1.008	0.984	1.016
1.023	0.977	1.047	0.953
1.012	0.988	1.023	0.977

Table 3.1: Mistuning patterns introduced

To give an idea of how just a 3% mistuning in stiffness or density can impact the system, here are reported two mode shapes of the tuned and mistuned systems:

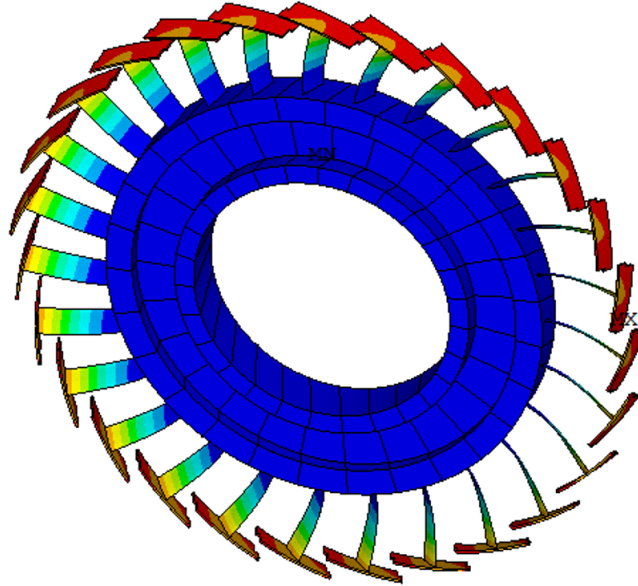


Figure 3.3: Example of tuned mode shape of the open contact system

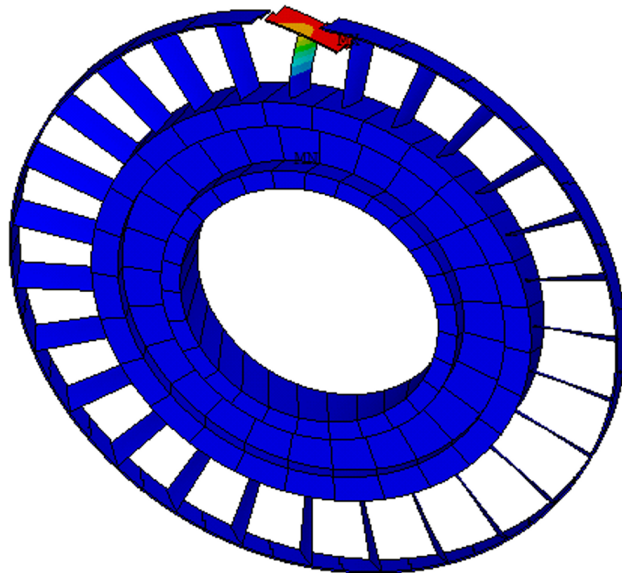


Figure 3.4: Example of mistuned mode shape of the open contact system

The localization of the vibration energy is evident in this case, while in the full stick cases it is much less immediate:

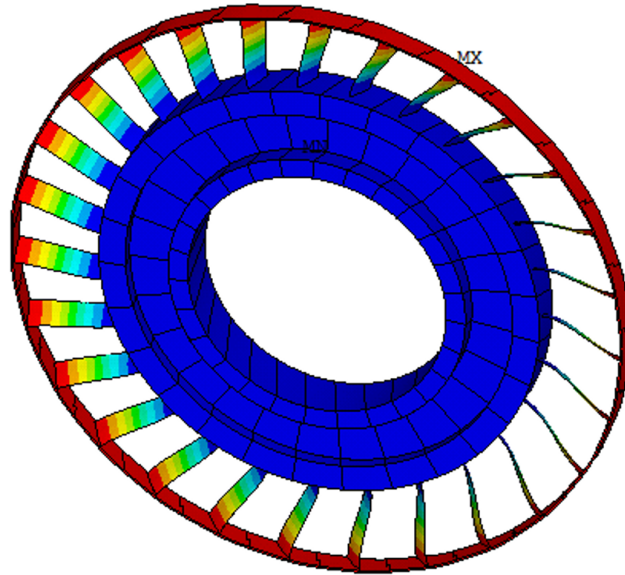


Figure 3.5: Example of tuned mode shape of the close contact system

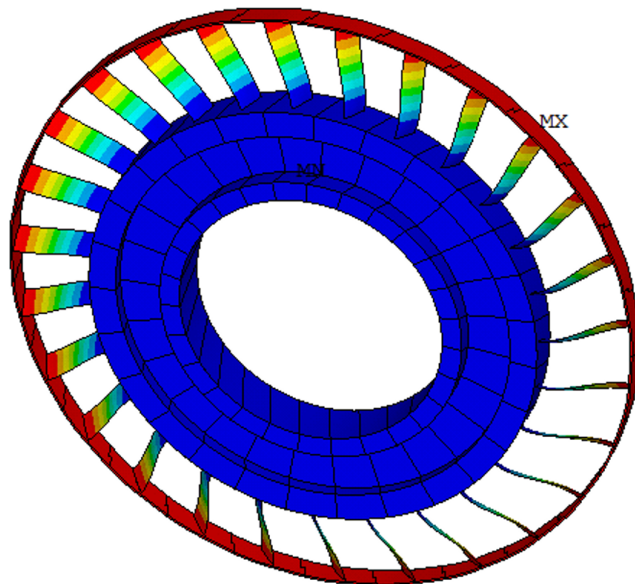


Figure 3.6: Example of mistuned mode shape of the close contact system

3.2 Tuned system characteristics

In this section will be presented the results obtained comparing the natural frequencies of the full system and the ROMs without the introduction of any mistuning.

In this section, as in the followings, will be distinguished two extreme cases: one with the contacts at the shroud interfaces completely open and one with the contact completely clumped. In reality the contact at the shroud interfaces is non-linear and its accurate descriptions in the models goes beyond the porpoises of this thesis.

Here are presented the natural frequencies of the systems at various harmonic indexes as obtained from a modal analysis performed in Ansys:

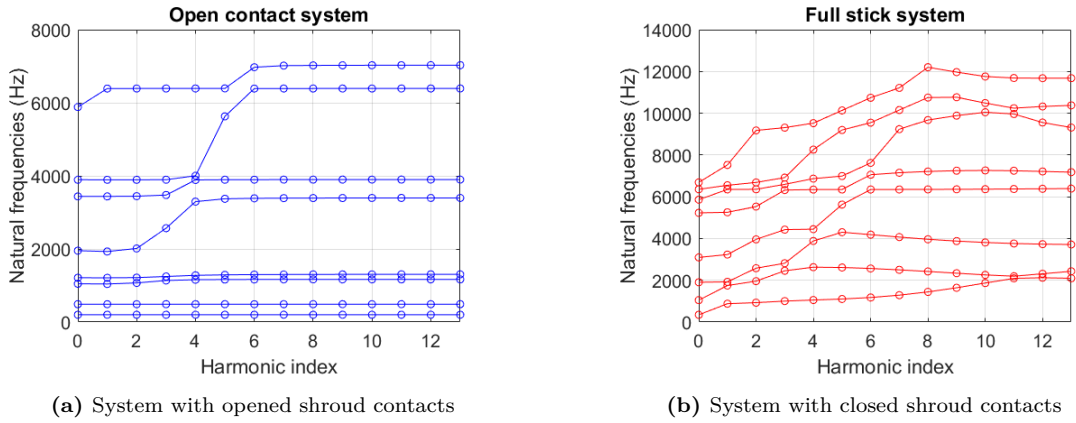


Figure 3.7: Natural frequencies at various harmonic indexes for the tuned systems

It is possible to see how the first families of mode shapes of the open contact's system are well distinguished from one another, however the close contact's system graphs shows that the families tend to interact more since the beginning. It is also noticeable how the natural frequencies of the close contact's system are overall higher than the other system's, this is due to an increased stiffness of the system thanks to the clumping of the shroud interfaces.

The different tuned ROMs have been tested to check how accurately they can predict the natural frequencies of the full system:

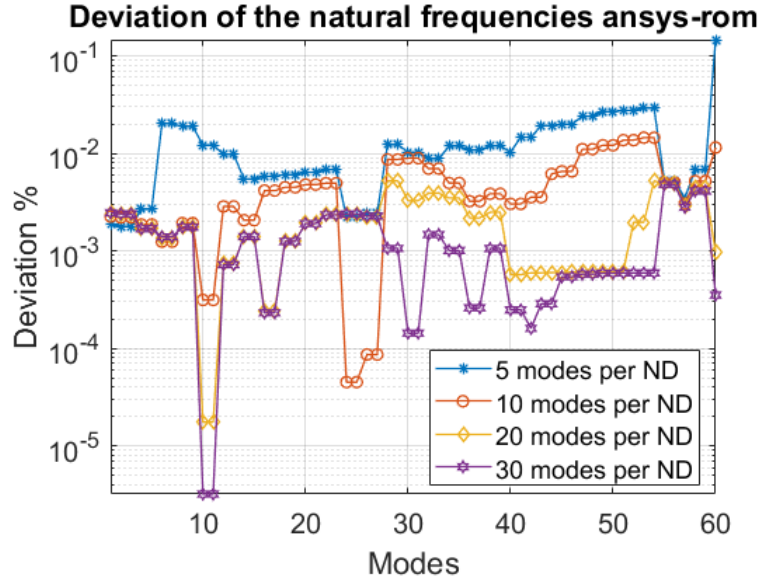


Figure 3.8: Deviation of the different tuned ROMs in predicting the natural frequencies

It is possible to see at what level the different ROMs can be considered precise in predicting higher natural frequencies. The precision of the ROMs is higher in the lowest natural frequencies range because of the set of retained full stick modes.

To increase the precision of the ROM it can be useful to retain a higher number of modes, but over a certain level the deviation doesn't decrease anymore.

3.3 Stiffness mistuning

In this section the performances of ROMs built introducing stiffness mistuning at different levels will be reported, considering 20 modes per harmonic index, which, as seen for the tuned case, is usually enough to have a converged ROM.

3.3.1 Natural frequencies

The first results shown refer to the open contact systems and intend on showing how accurate the prediction of the mistuned systems natural frequencies is.

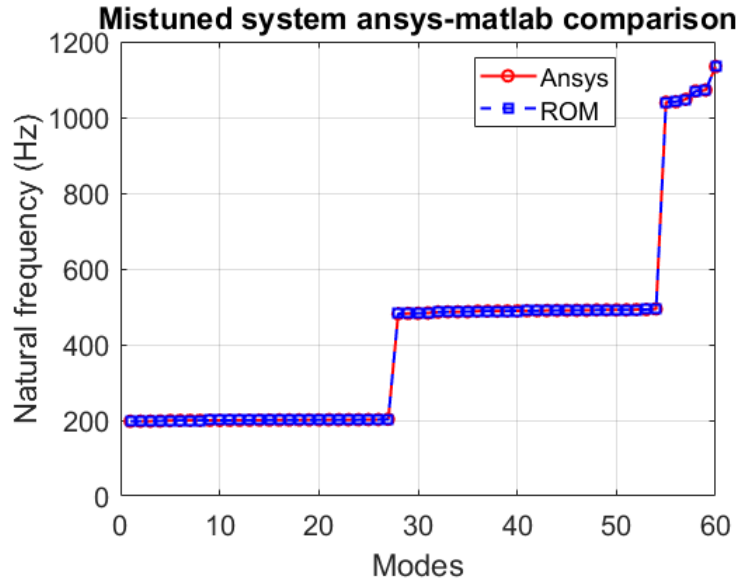


Figure 3.9: Natural frequencies of the open contact system, with 3% stiffness mistuning

The deviation between the Ansys model natural frequencies and the ones computed using the ROM is presented here:

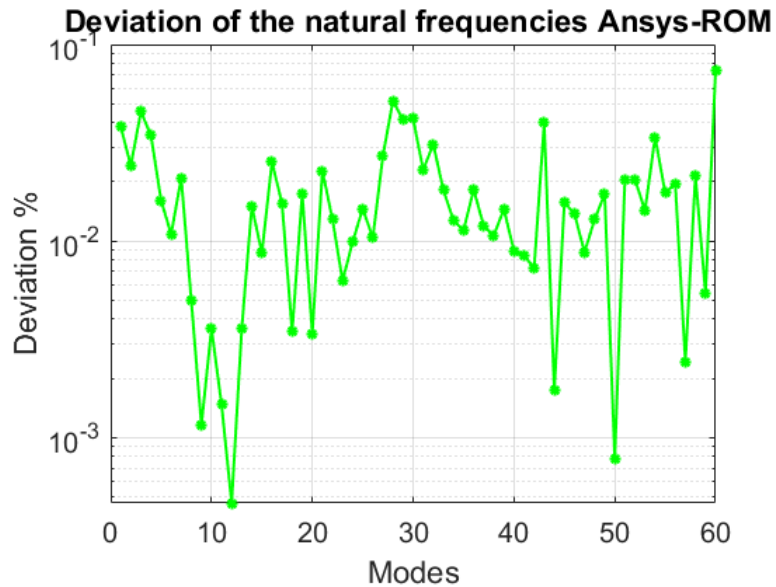


Figure 3.10: Deviation between the natural frequencies (Ansys-ROM) of the open contact system, with 3% stiffness mistuning

While considering the close contact systems, the results are:

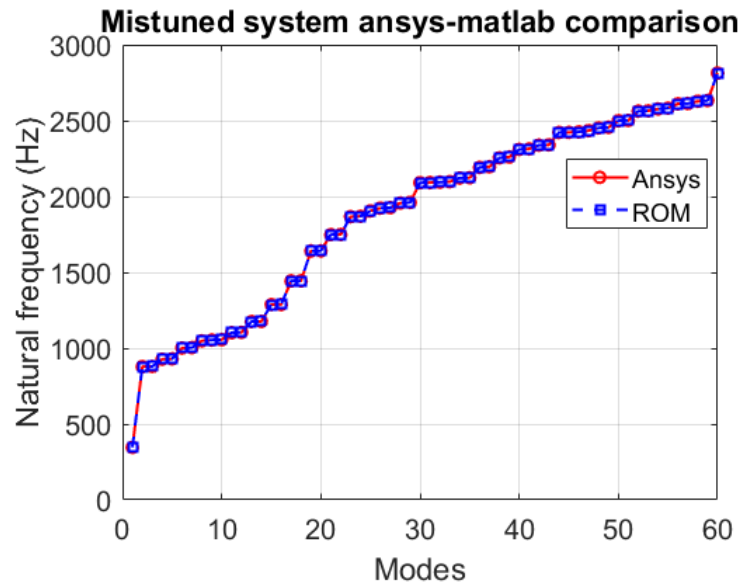


Figure 3.11: Natural frequencies of the close contact system, with 3% stiffness mistuning

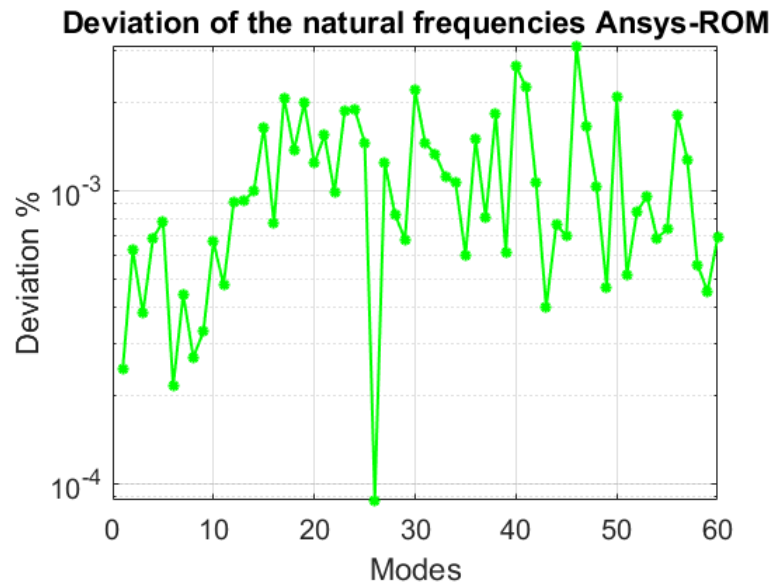


Figure 3.12: Deviation between the natural frequencies (Ansys-ROM) of the close contact system, with 3% stiffness mistuning

Increasing the severity of the mistuning to 6% deviation makes it harder for ROM to correctly predict the natural frequency, however the results are still accurate. Here are compared the deviations between the 3% and 6% mistuning for both the open and close cases.

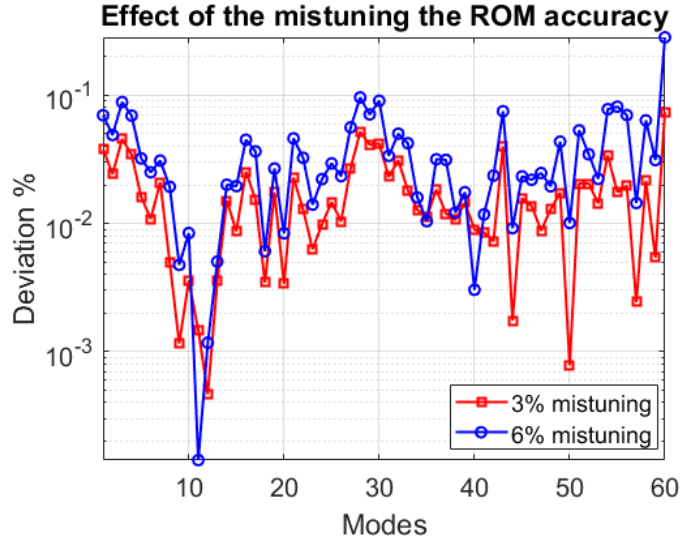


Figure 3.13: Comparison of the deviations between the 3% and 6% stiffness mistuned systems, open contact

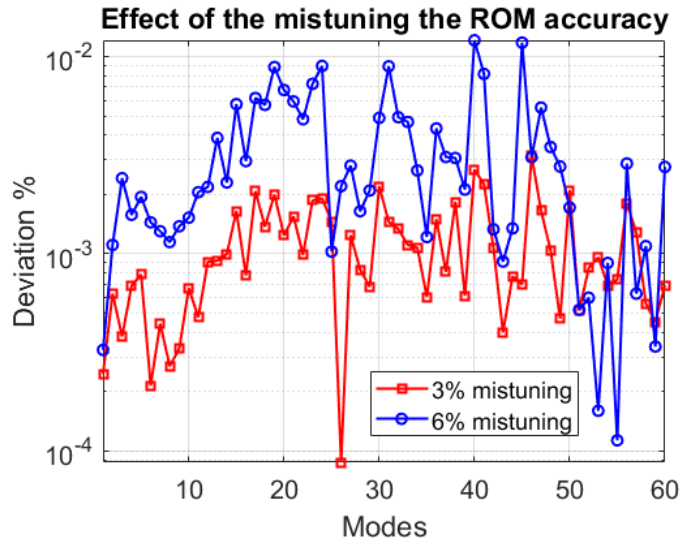


Figure 3.14: Comparison of the deviations between the 3% and 6% stiffness mistuned systems, close contact

It can also be noticed how the ROM perform better in predicting the close shroud system, this is due to the introduction, in the reduction basis, of the full stick modes.

3.3.2 Mode shapes

The mode shapes comparison has been performed using the Modal Assurance Criterion or MAC.

The comparison has been done considering the values of the mode shapes for the three DOFs of a node on the leading edge of the blades. The nodes considered are 27, one per sector, close to the shrouds. The choice was made trying to select a node that would present significant displacement for all the different mode shapes.

Starting with the open contact systems:

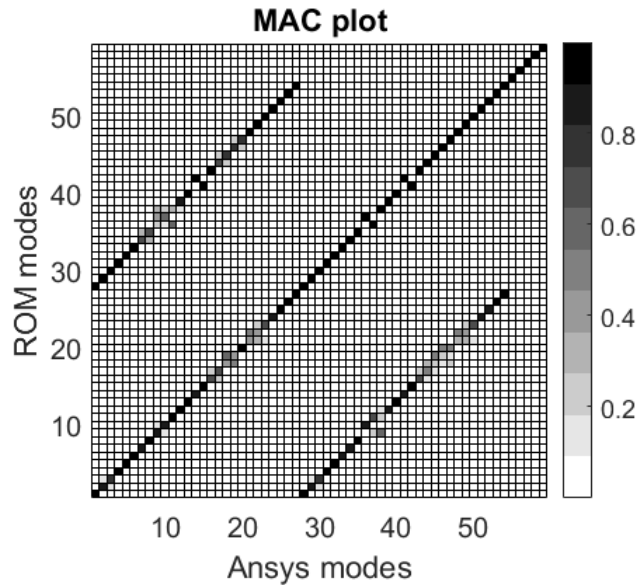


Figure 3.15: MAC plot for the open contact system with 3% stiffness mistuning

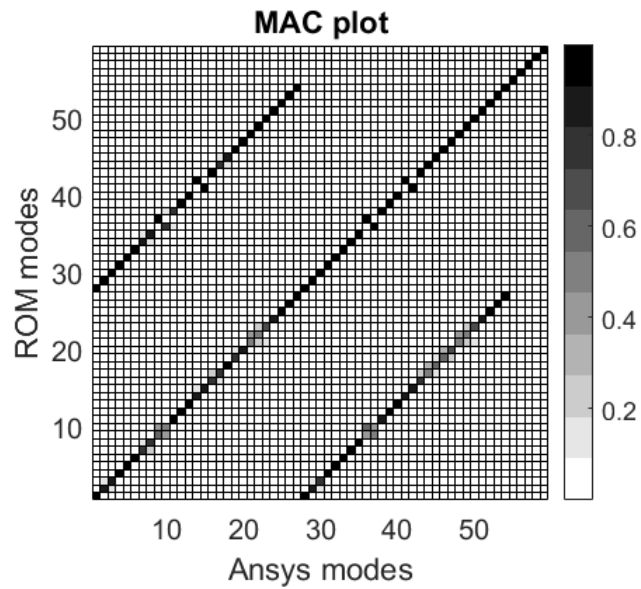


Figure 3.16: MAC plot for the open contact system with 6% stiffness mistuning

Both the Ansys mode shapes and the ROM mode shapes are ordered in ascending order of natural frequencies.

It is possible to notice how some mode shapes are predicted accurately but are ordered wrongly, this is due to the error in predicting the natural frequencies of two really close modes, which is large enough to switch their order.

In some other cases it is possible to identify small 2×2 matrices in the MAC matrices that show some deviation in predicting the mode shapes. For example here are shown the mode shapes of these cases for the open contact case with 3% mistuning:

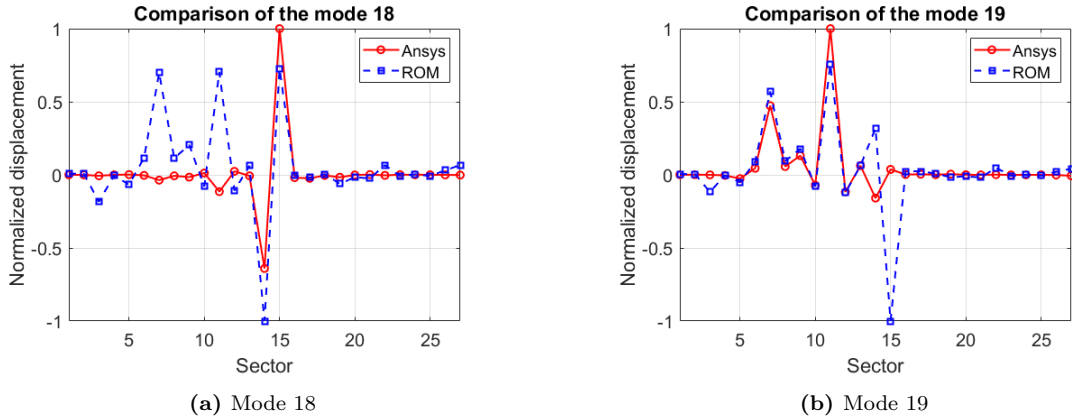


Figure 3.17: Normalized displacement of the chosen node in all sectors

It is possible to notice how the prediction of the ROM, mode by mode, has significant discrepancies with the Ansys results, but it has to be said that considering the two couples of mode shapes gives the same "information" in both cases, this means that the linear combinations of modes obtained from mode 18 and mode 19 in Ansys, can be also obtained as linear combinations of mode 18 and mode 19 of the ROM.

For the full stick cases the results obtained are:

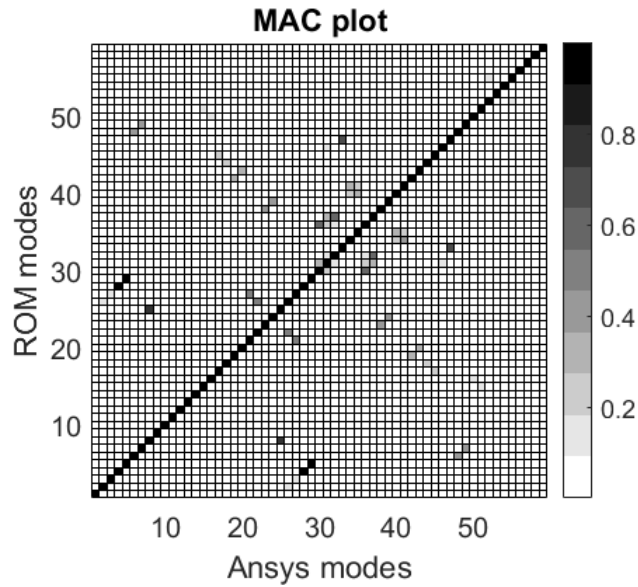


Figure 3.18: MAC plot for the full stick system with 3% stiffness mistuning

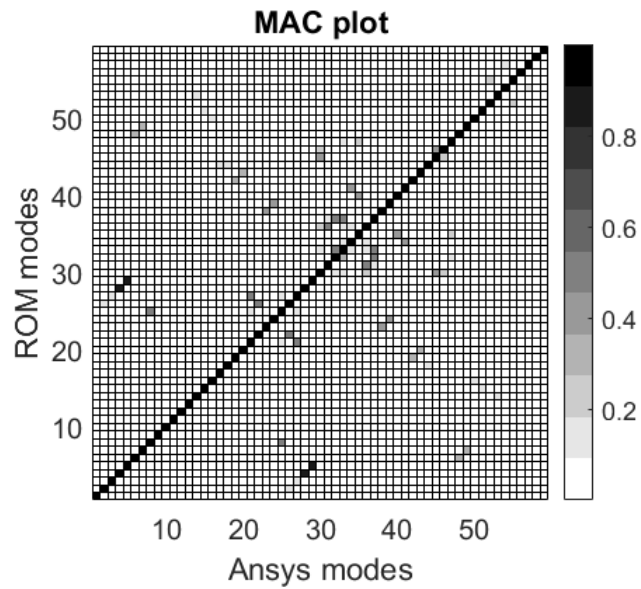


Figure 3.19: MAC plot for the full stick system with 6% stiffness mistuning

In this conditions the performance of the ROMs are better, since in the reduction process the base chosen contains the full stick mode shapes.

It is worth noticing one generic mode shape of the close contact case with 3% mistuning:

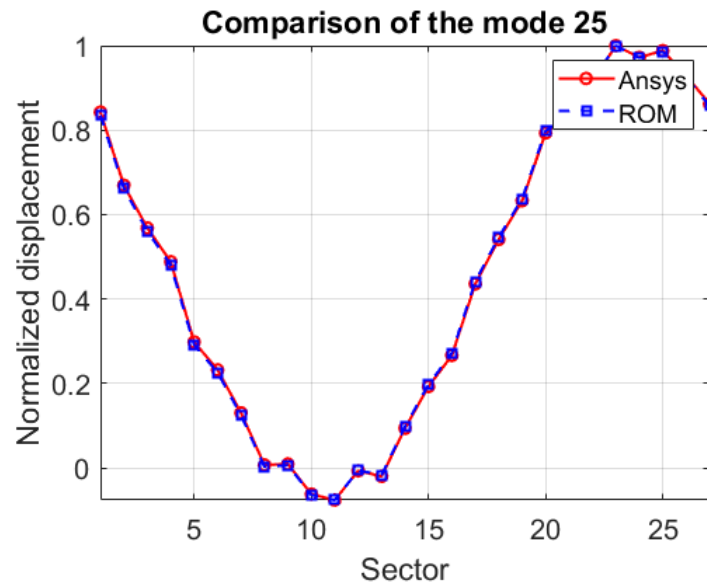


Figure 3.20: Normalized displacement of the chosen node in all sectors, mode 25

The full stick case's mode shapes maintain their periodicity and are overall much less impacted by the presence of mistuning thanks to the stiffening effect of the shrouds that also help transferring the vibration energy between the adjacent sectors. They tend to avoid the really localized mode shapes typical of the bladed disks with cantilever blades.

3.3.3 Linear forced response

The linear forced response was analyzed only for the full stick systems, this cases are more significant because the real micro-slip conditions of the shrouds contact interfaces are much closer to the close contact case than to the open contact one.

The force is applied at a node on top of the shrouds of every sector in a tangential direction. The magnitude of the forces is set to 100 N and the phase angles are known once engine order (EO) is defined. The amplitude of the response represented in the following results is relative to the tangential displacement of one node positioned on the blade close to the shroud. It was also considered a damping matrix defined as proportional to the stiffness matrix.

The range for the analysis, 2.000 Hz to 2.400 Hz and the EO, 11, were chosen based on the distribution of the natural frequencies of the tuned system at the various harmonic indexes (figure 3.7b):

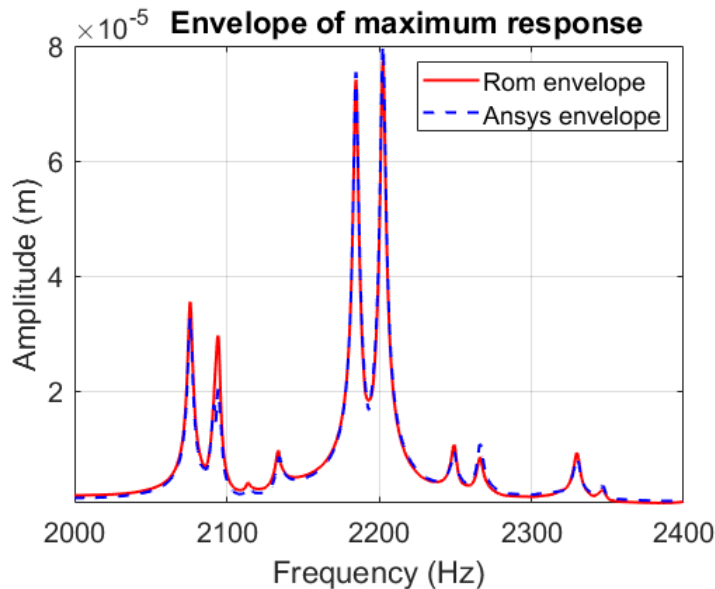


Figure 3.21: Envelope of maximum response for the full stick system with 3% stiffness mistuning, EO = 11

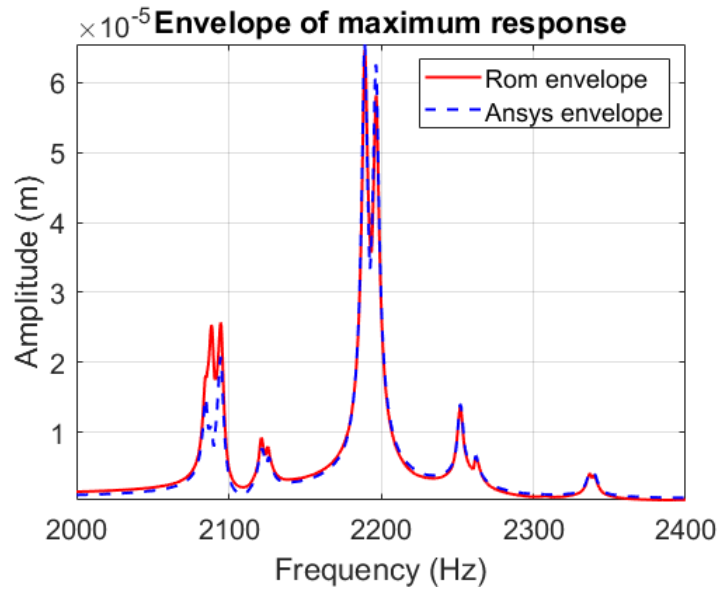


Figure 3.22: Envelope of maximum response for the full stick system with 6% stiffness mistuning, $EO = 11$

It is possible to observe how all the higher picks are correctly represented in the analysis, however in some of the smaller ones the ROMs tend to overestimate the response of the system.

3.4 Density mistuning

The procedure followed here will be the exact same as for the stiffness mistuning, in the following section will then be highlighted the differences and similarities between the two approaches.

3.4.1 Natural frequencies

The overall values of the natural frequencies for the stiffness and density mistuned systems are the same as it shown in figures A.1 and A.2, in this section will only be presented the results in terms of deviations and not in terms of absolute values because they would be redundant.

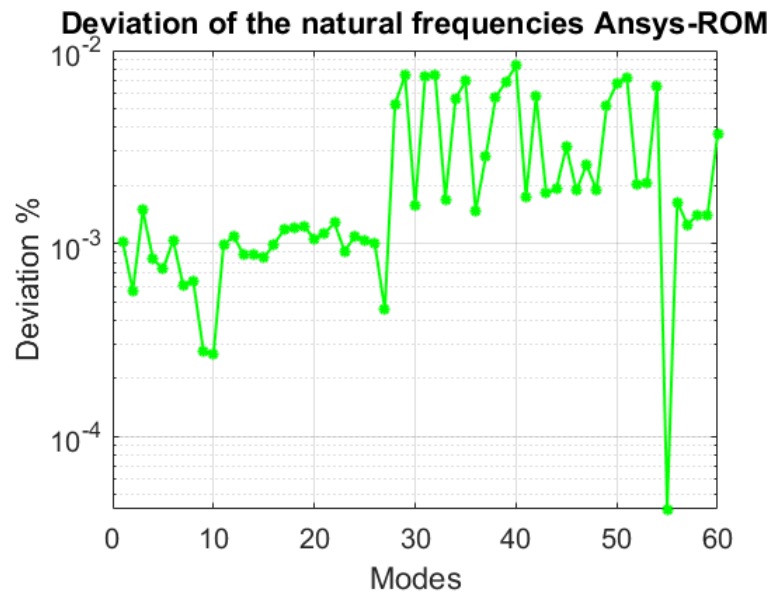


Figure 3.23: Deviation between the natural frequencies (Ansys-ROM) of the open contact system, with 3% density mistuning

While considering the close contact systems, the results are:

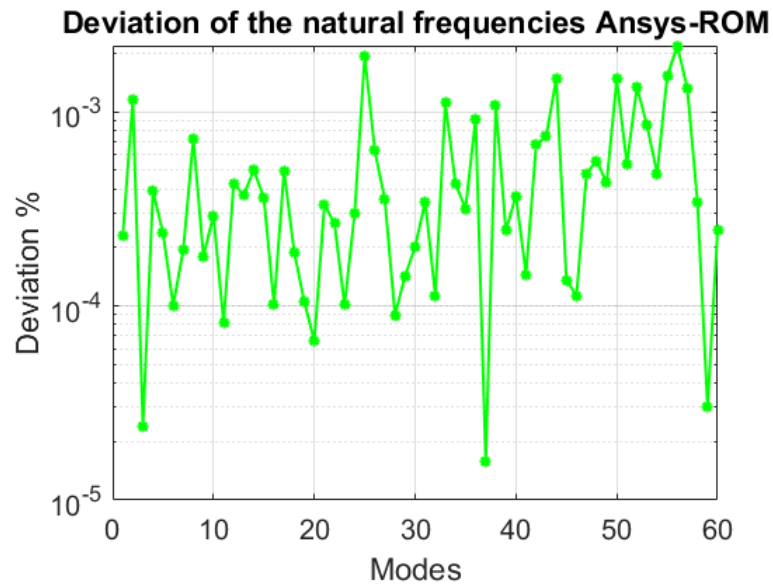


Figure 3.24: Deviation between the natural frequencies (Ansys-ROM) of the close contact system, with 3% density mistuning

The considerations made for the stiffness case are still valid: the severity of the mistuning impact the accuracy of the ROMs, but a 6% standard deviation pattern still gives good results for the first natural frequencies.

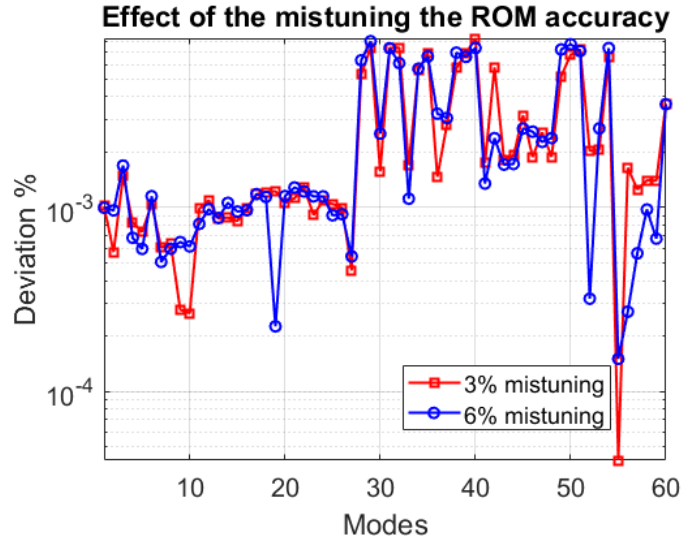


Figure 3.25: Comparison of the deviations between the 3% and 6% density mistuned systems, open contact

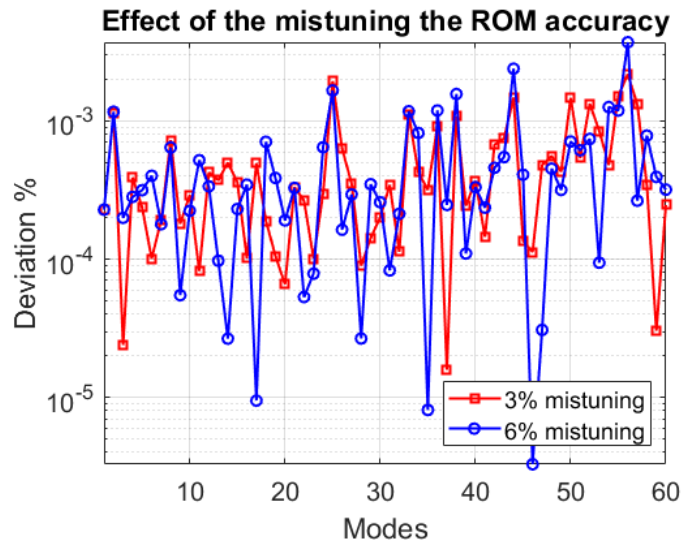


Figure 3.26: Comparison of the deviations between the 3% and 6% density mistuned systems, close contact

Comparing these results with the stiffness mistuning cases, it is possible to notice how the ROMs now maintain the same performances also in the 6% mistuning cases. Introducing mistuning in terms of density allows for better results in terms of natural frequencies also with more severe mistuning introduced.

3.4.2 Mode shapes

The comparison has been done considering the values of the mode shapes for the three DOFs of a node on the leading edge of the blades. The nodes considered are 27, one per sector, close to the shrouds. The choice was made trying to select a node that would present significant displacement for all the different mode shapes.

The open contact systems results are:

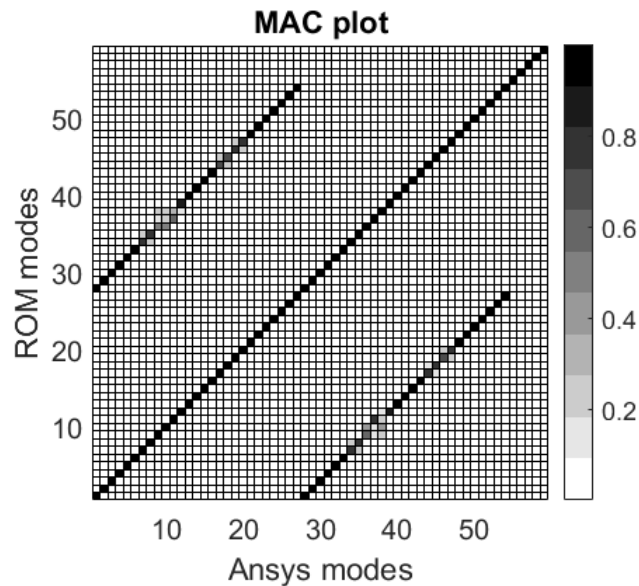


Figure 3.27: MAC plot for the open contact system with 3% density mistuning

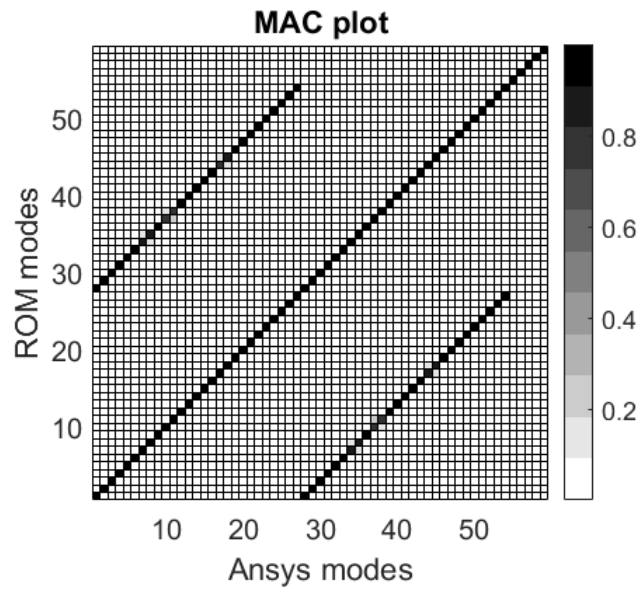


Figure 3.28: MAC plot for the open contact system with 6% density mistuning

Both the Ansys mode shapes and the ROM mode shapes are ordered in ascending order of natural frequencies.

In the close contact case, the MAC plots are:

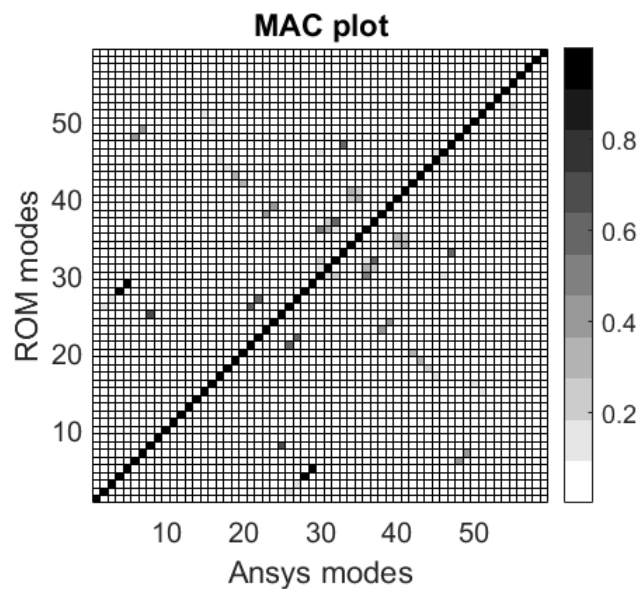


Figure 3.29: MAC plot for the close contact system with 3% density mistuning

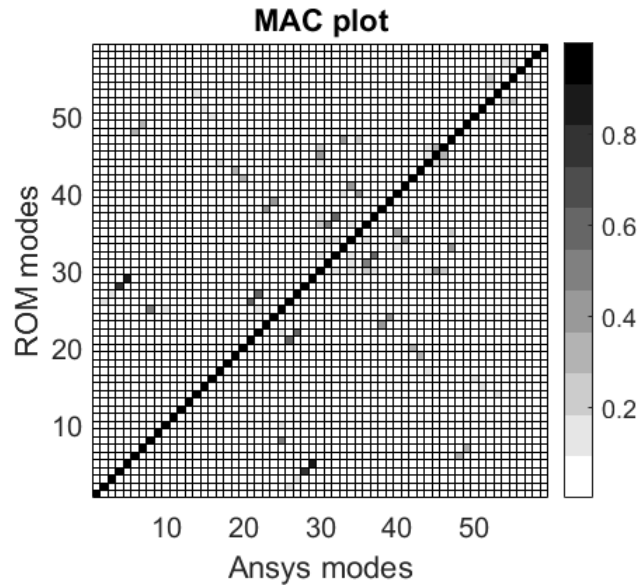


Figure 3.30: MAC plot for the close contact system with 6% density mistuning

According with what is presented in appendix A, the mode shapes of the density and stiffness mistuned systems are really similar thanks to how the mistuning pattern were chosen. Thanks to this, the phenomena described in the subsection 3.3.2 are still apparent in this case.

3.4.3 Linear forced response

In the density mistuning section as well, the linear forced response was analyzed only for the full stick systems.

The force is applied at a node on top of the shrouds of every sector in a tangential direction. The magnitude of the forces is set to 100 N and the phase angles are known once engine order (EO) is defined. The amplitude of the response represented in the following results is relative to the tangential displacement of one node positioned on the blade close to the shroud. It was also considered a damping matrix defined as proportional to the stiffness matrix.

The range for the analysis, 2.000 Hz to 2.400 Hz and the EO, 11, were chosen based on the distribution of the natural frequencies of the tuned system at the various harmonic indexes (figure 3.7b):

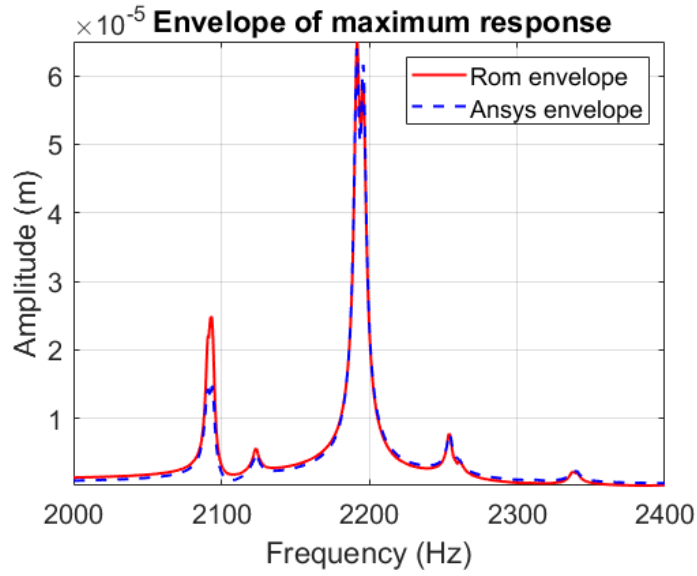


Figure 3.31: Envelope of maximum response for the full stick system with 3% density mistuning, $EO = 11$

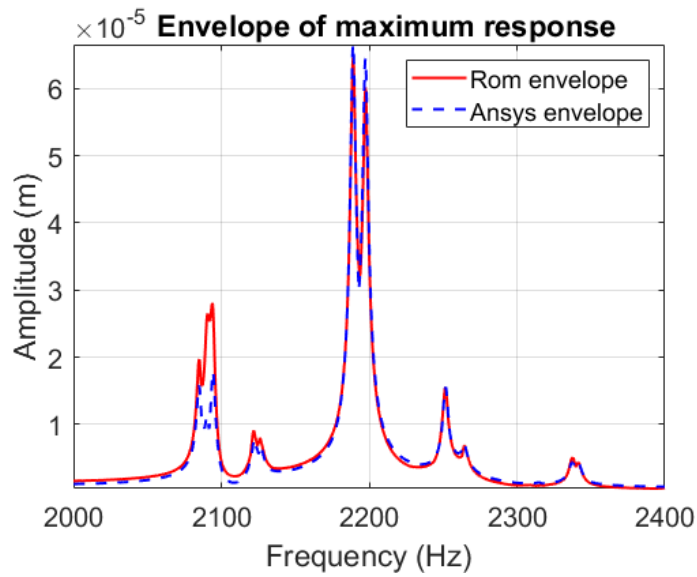


Figure 3.32: Envelope of maximum response for the full stick system with 6% density mistuning, $EO = 11$

It is possible to observe how all the higher picks are correctly represented in the analysis, however in some of the smaller ones the ROMs tend to overestimate the response of the system.

3.5 Performances comparison between density and stiffness mistuning

In this section are going to be compared the performances of the stiffness and density mistuning, in particular it will be shown how the different parameters considered in the previous results affect differently the accuracy of the ROMs.

It is noticeable to see how the accuracy of the ROMs in predicting the natural frequencies is impacted by the ROM size:

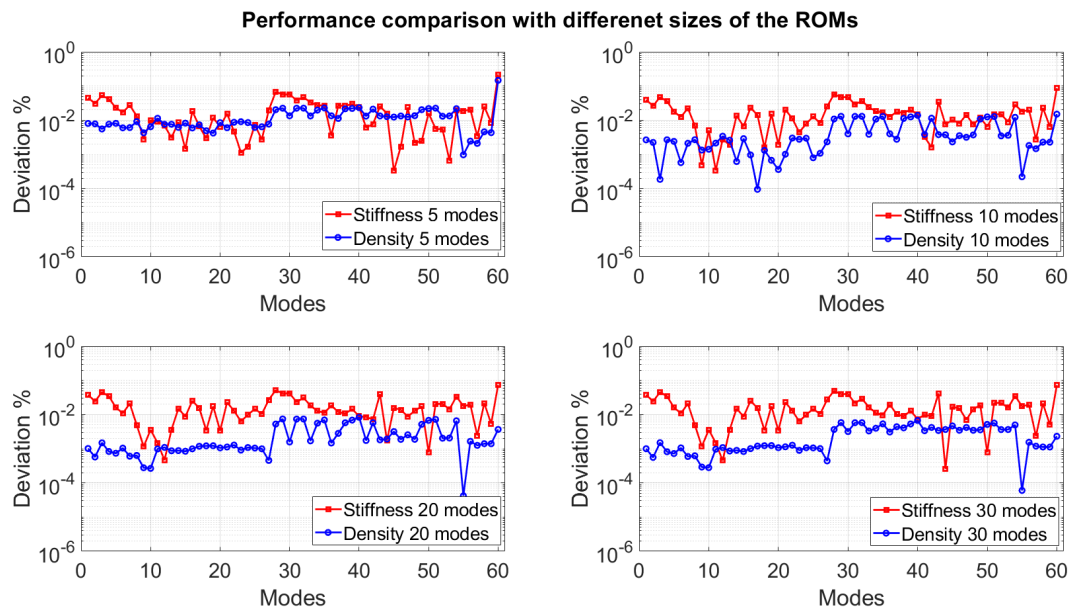


Figure 3.33: Accuracy in predicting the natural frequencies of the open contact systems, considering different ROMs sizes

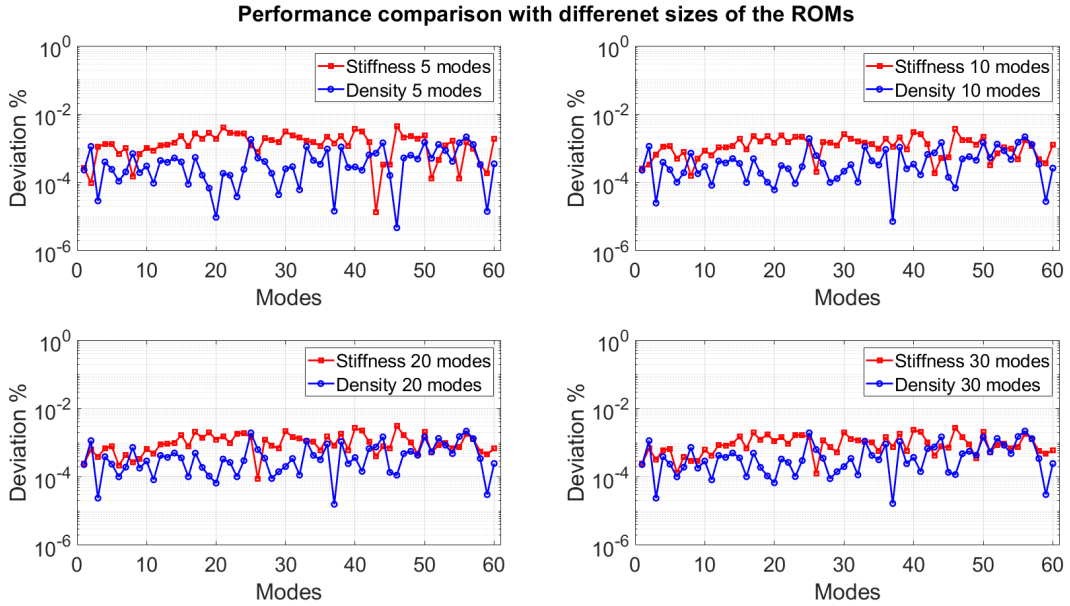


Figure 3.34: Accuracy in predicting the natural frequencies of the close contact systems, considering different ROMs sizes

This results are about the 3% mistuning ROMs. The deviations of the close cases are comparable for all the ROMs sizes, this was expected since in this systems the constraint modes are not playing any role and the accuracy of the ROMs is only dependent on the full stick modes. In the open contact case however, the performances of the density mistuned ROMs improve far better, with the size of the matrices, than the the stiffness mistuned ones. In this case, the introduction of density mistuning, which allows for exact constraint modes, represents the better option.

The same comparison can be performed with the diagonal of the MAC matrix, to see how the different types of mistuning can approximate the mode shapes. It must be specified that for this comparison it was considered the highest value of three central diagonals of the MAC matrices, to make sure that the wrong ordering of the mode shapes doesn't affect the results presented.

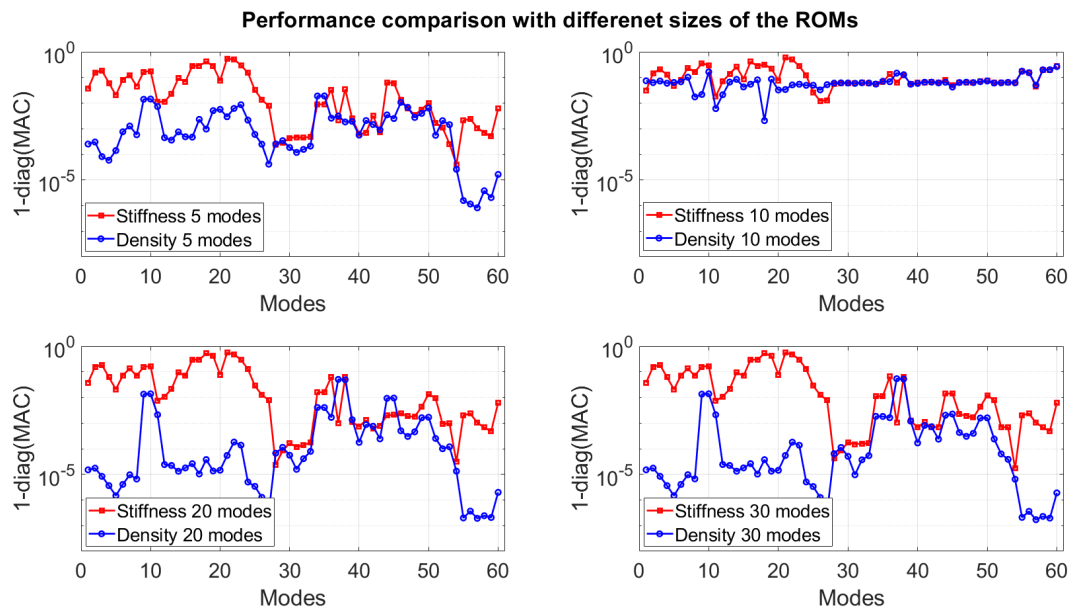


Figure 3.35: Accuracy in predicting the mode shapes of the open contact systems, considering different ROMs sizes

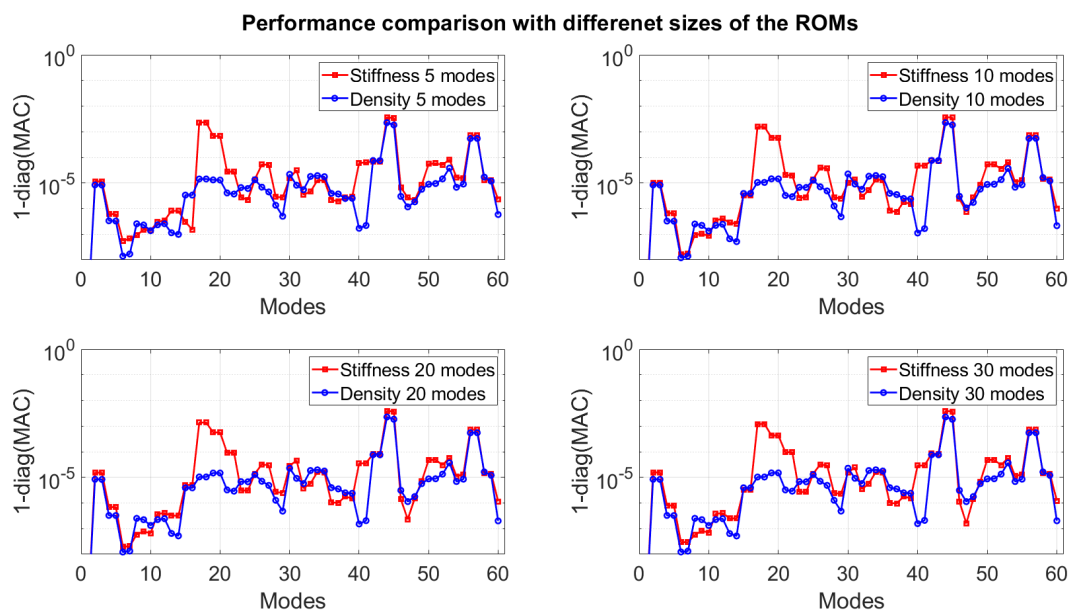


Figure 3.36: Accuracy in predicting the mode shapes of the close contact systems, considering different ROMs sizes

3.5. PERFORMANCES COMPARISON BETWEEN DENSITY AND STIFFNESS MISTUNING

Once again the results for the close contact systems are overall better, but there is no significant difference in introducing either stiffness or density mistuning, while for the open contact systems the density mistuned ROMs are more precise than the stiffness mistuned ones.

Chapter 4

Conclusions

This thesis presented the computational implementation of the RCCMS method described in [1], developing the algebra involved in details. Closing the Methodology chapter, it is presented the introduction of mistuning in the final reduced order models, highlighting the differences between stiffness and density mistuning from the algebraic point of view, however both can be introduced with ease making the method suitable for industrial applications where statistical analysis are required for the characterization of bladed disks.

In the Results chapter are presented the most significant results of the tests operated on the various ROMs generated. The systems have been tested considering the accuracy in predicting the natural frequencies, the mode shapes and the linear forced response of a FE model available in Ansys.

The tests showed how it is equivalent to introduce the mistuning in terms of stiffness or density if the behaviour of the bladed disk is close to a full stick condition, where the contact interfaces at the blades shrouds have no relative displacement between adjacent sectors. However, the more the system's behaviour can be represented as a bladed disk with cantilever blades, the more introducing density mistuning is convenient compared to stiffness mistuning. The behaviour of the system is, in reality, non-linear and depends on multiple factors like pre-stress applied at the shrouds and friction coefficient between the shrouds interfaces. It is necessary then to perform a non-linear forced response analysis, comparing the results given by the ROMs and a finite element model, to further investigate if the density mistuning can, indeed, be a suitable alternative to stiffness mistuning.

Bibliography

- [1] S. Mehrdad Pourkiaee. *Models and Experiments for Nonlinear Dynamics of Mistuned Bladed Disks with Friction Contacts*. 2020 (cit. on pp. [2](#), [19](#), [49](#)).
- [2] Andrew Madden, Bogdan I. Epureanu, and Sergio Filippi. *Reduced-Order Modeling Approach for Blisks with Large Mass, Stiffness, and Geometric Mistuning*. 2012 (cit. on p. [10](#)).
- [3] Brian J. Olson, Steven W. Shaw, Chengzhi Shi, Christophe Pierre, and Robert G. Parker. *Circulant Matrices and Their Application to Vibration Analysis*. 2014 (cit. on p. [15](#)).
- [4] S. Mehrdad Pourkiaee, Stefano Zucca, and Robert G. Parker. *Relative cyclic component mode synthesis: A reduced order modeling approach for mistuned bladed disks with friction interfaces*. 2022 (cit. on p. [16](#)).
- [5] S. Mehrdad Pourkiaee, Stefano Zucca, and Robert G. Parker. *Relative cyclic component mode synthesis and its application to nonlinear vibration analysis of mistuned bladed disks with friction joints*. 2018.
- [6] Stefano Zucca. *Slide del corso di Dinamica dei rotori per applicazioni aerospaziali*. 2021.

Appendix A

Comparison of the stiffness and density mistuned systems

In this appendix will be addressed the validity of the hypotheses that the two systems generated with the δ mistuning patterns defined using equation 3.1, are, in fact, similar in terms of natural frequencies and mode shapes. The results presented here are referred only to the 3% mistuning cases for brevity.

A.1 Natural frequencies

The comparisons presented here are all between FE models, which are the ones used as references to show the performances of the ROMs. The first graphs show how close the natural frequencies of the density and stiffness mistuned systems are. The figure A.1 refers to the systems with open contact at the shrouds interfaces, while the figure A.2 refers to the system in full stick conditions.

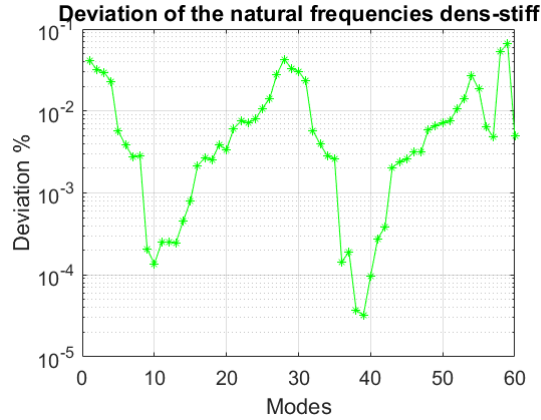


Figure A.1: Natural frequencies deviation between the stiffness and density mistuned open contact systems

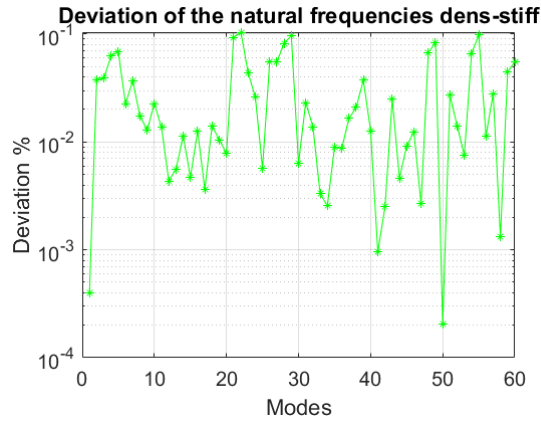


Figure A.2: Natural frequencies deviation between the stiffness and density mistuned closed contact systems

For both cases the deviation between the first natural frequencies of the systems never exceeds 0.1%.

A.2 mode shapes

As in the other cases the mode shapes comparison is performed using the modal assurance criterion (MAC), evaluating how similar the modes of the two mistuned systems are. The comparison was performed using only the values of the mode shapes for one node (three degrees of freedom). As for the natural frequencies, both

cases are presented. The figure A.3 refers to the systems with open contact at the shrouds interfaces, while the figure A.4 refers to the system in full stick conditions.

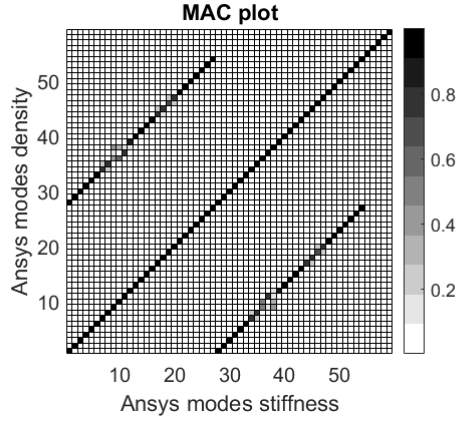


Figure A.3: mode shapes comparison between the stiffness and density mistuned open contact systems

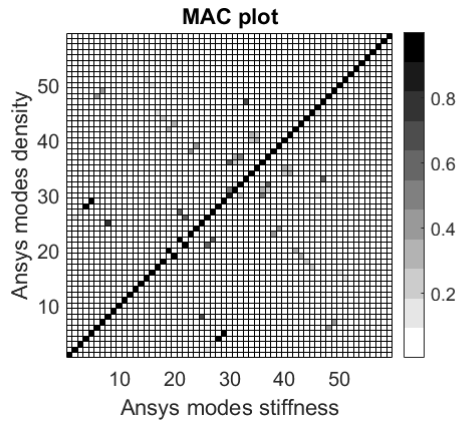


Figure A.4: mode shapes comparison between the stiffness and density mistuned closed contact systems

For the open contact case it is possible to see how there is close to perfect match between the various mode shapes, while for the closed contact case few modes are ordered differently but, a part from that, the results are really close. The results presented in this chapter show how the introduction of the mistuning in terms of a vector of δ_n , which is applied as it is to the stiffness and after the transformation in equation 3.1, to the density, guarantees good similarity between the systems generated.